PNAS
www.pnas.org

Supplementary Information for

Yeast ATM and ATR use different mechanisms to spread histone H2A phosphorylation around a DNA double-strand break

Kevin Li[1], Gabriel Bronk[1], Jane Kondev[1] and James E. Haber[2]

[1]Department of Physics, Brandeis University, Waltham, MA

[2]Department of Biology and Rosenstiel Basic Medical Sciences Research Center, Brandeis University, Waltham, MA

Corresponding authors: James E. Haber and Jane Kondev

Email: haber@brandeis.edu, kondev@brandeis.edu

This PDF file includes:

- Supplementary text
- Figures S1-S19
- Tables S1-S5
- Description of Dataset S1
- References for Supplementary Information

Other supplementary materials for this manuscript:

- Dataset S1

www.pnas.org/cgi/doi/10.1073/pnas.2002126117

Table of Contents

Supplementary Text……………………………………………………………………..3

Experimental Methods………………………………………………………………….....3

Model Derivations……………………………………………………………………….....4

DSB Formation……………………………………………………………………………4

Directed Sliding Model Derivation……………………………………………………..4

Looping Model Derivation………………………………………………………………...8

1D Diffusion Model Simulation…………………………………………………………13

3D Diffusion Model Derivation…………………………………………………………15

Accounting for γ-H2AX Measurements near the Recombination Enhancer……………..18

Some Models Require Kinase Activation at the DSB……………………………………19

A Quantitative Model of ChIP……………………………………………………………20

Basal γ-H2AX Levels are Incorporated into the Predicted ChIP Signals…………………23

A Quantitative Model of ChIP for the Directed Sliding Model…………………………..23

Bayes Factor Calculation…………………………………………………………………24

Supplemental Figures…………………………………………………………..……27

Supplemental Tables……………………………………………………………………46

Description of Supplemental Dataset ...…...…………………………………………..… 52

References for Supplementary Information…………………………………………..53

Supplementary Text

Experimental Methods

Strain construction

All strains used are a variant of the strain JKM139 (1). Strain JKM139 has the genotype *MAT***a** *hml*Δ::*ADE1 hmr*Δ::*ADE1 ade1-100 leu2-3,112 lys5 trp1*::*hisG' ura3-52 ade3::GAL::HO.*

*nej1*Δ::HPH mutants were constructed by amplifying pAG32 (HPH) using primers Nej1-MXp1 and Nej1-MXp2 and *yku80*Δ::HPH mutants were constructed by PCR-amplifying pJH1515 using primers ku80MX18 and ku80MX19 to create a fragment containing hygromycin-resistance with homology to *NEJ1* and *YKU80*, respectively. Linear DNA was introduced to the appropriate strain using lithium acetate transformation. *hta1-S129A* mutants were generated by transforming strains with pBL13, which contains *Cas9* and a gRNA targeting *HTA1*, and the repair template BL327. Similarly, *hta2-S129A* mutants were generated by transforming strains with pBL14, which contains *Cas9* and a gRNA targeting *HTA2*, and the repair template BL331. The exact primer sequences of the repair oligos are shown in Table S3. S129A mutations were confirmed through sequencing by GENEWIZ.

Ddc2 was overexpressed in strain yKL019 by integrating PML105.45 (obtained from Maria Pia Longhese) which carries a copy of *GAL1-Ddc2*. PML105.45 was cut overnight with *Cla*I and integrated at *leu2-3,112* by transformation.

Growth conditions and DSB induction

Cells from a single colony were grown overnight in 5 ml of YEPD, washed three times with YEP + 3% lactic acid (YEP-Lac) and then grown in 350 ml of YEP-Lac until log phase growth with a cell concentration between 5×10^6 cells/ml and 8×10^6 cells/ml. α-factor (United Biochemical) was added to the culture to a concentration of ~5 μM and maintained in the cell culture for at least for two doubling times before cell collection. G1 arrest was confirmed microscopically. After G1 arrest, 20% galactose was added to the YEP-Lac culture to a final concentration of 2% to induce *GAL*::*HO* expression, resulting in cutting at the *MAT***a** locus.

Chromatin immunoprecipitation

45 ml of culture were fixed and crosslinked with 1% formaldehyde for 10 min, after which 2.5 ml of 2.5 M glycine was added for 5 min to quench the reaction. Cells were pelleted and washed 3 times with 4°C TBS. Yeast cell walls were disrupted by beating the cells with 425-600 μm glass beads for 1 h in lysis buffer at 4°C. The lysate was sonicated for 2 min to obtain chromatin fragments of ~500 bp in length. Debris was then pelleted and discarded, and equal volume of lysate was immunoprecipitated using γ-H2AX antibody (abcam ab15083) for 1 h at 4°C, followed by addition of Protein-A agarose beads (Sigma-Aldrich #1719408001) for 1 h at 4°C. The immunoprecipitate was then washed twice in 140 mM NaCl lysis buffer, once with 0.5 M NaCl lysis buffer, once with 0.25 M LiCl wash buffer and once with TE. Crosslinking was reversed at 65°C overnight followed by proteinase-K and glycogen addition for 2 h. Protein and nucleic acids were separated by phenol extraction. LiCl was added to a final concentration of 400 mM LiCl. DNA was precipitated using 99.5% EtOH. A second precipitation step was carried out using 75% EtOH and the DNA resuspended in TE.

Model Derivations

All models are derived below and plotted in Figures S5-S16.

DSB Formation

All models begin with the formation of the DSB. We experimentally measure the cumulative probability distribution of the DSB formation time (Figure S1), and in all models we use this distribution by approximating it as a 12 minute lag time followed by the formation of the DSB at a rate of $k_{DSB} = 0.08/\text{minute}$.

Directed Sliding Model Derivation

Derivation Assuming a Kinase is at the Break Site at Time 0

We first derive a very simple model (in the next section we go on to a more detailed model, which is the one we compare to the experimental data). We model the chromosome as a 1D lattice of H2As: the H2As are at positions 1, 2, 3… and the break site is at position 0. The kinase is at position 0 at time 0 and then stochastically steps from one position to the next at a rate k_{slide}. At time t, the probability that the kinase is at position i is $((k_{slide}t)^i e^{-k_{slide}t})/i!$. This is simply the Poisson distribution.

Next we include the process of the kinase falling off the chromosome at a rate k_{off}, regardless of where on the chromosome the kinase is located. $e^{-k_{off}t}$ is the probability that the kinase is still on the chromosome at time *t*. $P_{kinase}(i,t)$, the joint probability that the kinase is still on the chromosome AND is at the *i*-th H2A at time *t,* is therefore given by the product of the Poisson distribution and $e^{-k_{off}t}$:

$$P_{kinase}(i,t) = \frac{(k_{slide}t)^i e^{-k_{slide}t}}{i!} e^{-k_{off}t} \tag{1}$$

$P_{phos}(i,t)$, the probability that the H2A at position *i* has been phosphorylated by time *t*, is given by

$$P_{phos}(i,t) = \sum_{j=i+1}^{\infty} P_{kinase}(j,t) + \int_0^t k_{off} \sum_{j=i+1}^{\infty} P_{kinase}(j,z)\,dz \tag{2}$$

This formula follows from the assumption that the kinase phosphorylates every H2A that it comes to. Hence, if at time *t* the kinase is currently on an H2A at any position $j > i$, then we know that the kinase has already been to the *i*-th H2A and has already phosphorylated it. The first term in equation (2) is the probability that at time *t* the kinase is currently at any location beyond position *i*. (The summation goes to infinity for mathematical simplicity. Because $P_{kinase}(j,t)$ is small at large *j,* there would be little change if we used a summation limit equal to the actual number of H2As in the chromosome). Similarly, if the kinase has fallen off the chromosome from any position $j > i$ at any time before *t*, then we know that the *i*-th H2A has already been phosphorylated. The second term in equation (2) is the probability that the kinase has fallen off the chromosome from anywhere beyond position *i* at any time before time *t*.

Next we simplify the summation term in equation (2):

$$\sum_{j=i+1}^{\infty} P_{kinase}(j,t)$$

$$= e^{-k_{off}t} \sum_{j=i+1}^{\infty} \left(\frac{(k_{slide}t)^j e^{-k_{slide}t}}{j!} \right)$$

$$= e^{-k_{off}\,t}\left(1-\sum_{j=0}^{i}\left(\frac{(k_{slide}t)^j\,e^{-k_{slide}\,t}}{j!}\right)\right)$$

$$= e^{-k_{off}\,t}\,\frac{\gamma\left(i+1,\,k_{slide}t\right)}{\Gamma\left(i+1\right)} \tag{3}$$

where Γ is the complete gamma function, and γ is the lower incomplete gamma function. Plugging expression (3) into equation (2), we obtain

$$P_{phos}(i,t) = e^{-k_{off}\,t}\,\frac{\gamma\left(i+1,\,k_{slide}t\right)}{\Gamma\left(i+1\right)} + \int_0^t k_{off}\,e^{-k_{off}\,z}\,\frac{\gamma\left(i+1,\,k_{slide}z\right)}{\Gamma\left(i+1\right)}dz \tag{4}$$

After evaluating the integral and simplifying, we obtain

$$P_{phos}(i,t) = \frac{(1-q)^{i+1}}{\Gamma(i+1)}\left[i\,\gamma\left(i,\,k_{move}t\right)-[k_{move}t]^i\,e^{-k_{move}t}\right] \tag{5}$$

where $q=\dfrac{k_{off}}{k_{slide}+k_{off}}$ and $k_{move}=k_{slide}+k_{off}$.

Derivation that Incorporates the Variability in the Timing of DSB Formation and Arrival of the Kinase to the Break Site

Until this point, we have said that at $t = 0$ the kinase is at the break site and begins sliding along the chromosome. However, in different cells in the yeast population, the kinase starts sliding at different times (this will be detailed below). For an individual yeast cell, let τ be the time when the kinase begins the sliding process – i.e. the kinase does exactly what we described and derived so far, but beginning at time τ rather than time 0. Thus, we write $P_{phos}(i,t\mid\tau)$, which is the probability that the H2A at position *i* has been phosphorylated by time *t*, given that the kinase began the sliding process at time τ:

$$P_{phos}(i,t\mid\tau)=\begin{cases}\dfrac{(1-q)^{i+1}}{\Gamma(i+1)}\left[i\,\gamma\left(i,\,k_{move}(t-\tau)\right)-[k_{move}(t-\tau)]^i\,e^{-k_{move}(t-\tau)}\right], & \text{when } t\geq\tau\\ 0, & \text{when } t<\tau\end{cases} \tag{6}$$

The sliding start time is stochastic and is described by the probability density function $PDF(\tau)$, which is derived in the following manner: The chromosome begins intact, which we call state I. The DSB forms at a rate k_{DSB}: the chromosome is said to be in state II when there is a DSB but the kinase is not yet sliding. We make the assumption that once a yeast cell has a DSB, there is a single rate-limiting step described by the rate k_{init} that determines how soon the kinase initiates the sliding process (i.e. how soon the kinase arrives to the break site and then leaves the break site to slide along the chromosome). As soon as the kinase begins the sliding process, the chromosome is said to be in state III. Thus, k_{DSB} is the transition rate from state I to state II, and k_{init} is the transition rate from state II to III; this is captured by the coupled differential equations and initial conditions (7). (To simplify the derivation of the sliding model, in each yeast cell we say that only one copy of the kinase arrives at the break site; additional copies would have little effect on the predicted γ-H2AX profile because this derivation assumes that the kinase phosphorylates every H2A that it comes to). Let the functions $I(t)$, $II(t)$, and $III(t)$ represent the probabilities of being in states I, II, and III, respectively. We have

$$\begin{aligned} \frac{dI(t)}{dt} &= -k_{DSB}I(t) & I(0) &= 1 \\ \frac{dII(t)}{dt} &= k_{DSB}I(t) - k_{init}II(t) & II(0) &= 0 \\ \frac{dIII(t)}{dt} &= k_{init}II(t) & III(0) &= 0 \end{aligned} \tag{7}$$

$PDF(\tau)$ is the probability per unit time that a cell will enter the state in which the kinase is sliding (i.e. state III). Therefore, $PDF(\tau) = \frac{dIII}{dt}$. Solving equations (7) we obtain

$$PDF(\tau) = \frac{k_{init}k_{DSB}}{k_{init} - k_{DSB}}\left(e^{-k_{DSB}\tau} - e^{-k_{init}\tau}\right) \tag{8}$$

We calculate $P_{phos}(i,t)$, the probability that the H2A at position i has been phosphorylated by time t, where the time when the kinase begins the sliding process is distributed according to equation (8). $P_{phos}(i,t)$ is given by the integral of the product of equations (5) and (8):

$$P_{phos}(i,t) = \int_0^t P_{phos}(i,t \mid \tau) PDF(\tau)\, d\tau \tag{9}$$

Evaluating this integral gives

$$\begin{aligned}
P_{phos}(i,t) = \frac{(1-q)^{i+1}}{k_{init}-k_{DSB}} \Bigg[& k_{init} \Bigg(\frac{\gamma(i,k_{move}t)}{\Gamma(i)} + \frac{e^{-k_{move}t}t^{i-1}k_{move}{}^{i}}{\Gamma(i)(k_{move}-k_{DSB})} \\
& - \frac{e^{-k_{DSB}t}k_{move}{}^{i}}{(k_{move}-k_{DSB})^{i}} \left[\frac{\gamma\big(i+1,(k_{move}-k_{DSB})t\big)k_{DSB}}{\Gamma(i+1)(k_{move}-k_{DSB})} + \frac{\gamma\big(i-1,(k_{move}-k_{DSB})t\big)}{\Gamma(i-1)} \right] \Bigg) \\
& - k_{DSB} \Bigg(\frac{\gamma(i,k_{move}t)}{\Gamma(i)} + \frac{e^{-k_{move}t}t^{i-1}k_{move}{}^{i}}{\Gamma(i)(k_{move}-k_{init})} \\
& - \frac{e^{-k_{init}t}k_{move}{}^{i}}{(k_{move}-k_{init})^{i}} \left[\frac{\gamma\big(i+1,(k_{move}-k_{init})t\big)k_{init}}{\Gamma(i+1)(k_{move}-k_{init})} + \frac{\gamma\big(i-1,(k_{move}-k_{init})t\big)}{\Gamma(i-1)} \right] \Bigg) \Bigg]
\end{aligned}$$

(10)

Looping Model Derivation

We model the chromosome as an unconfined worm-like chain at thermodynamic equilibrium. Similar polymer models have also accurately predicted contact frequencies as well as the 3D positioning of genes in the yeast nucleus (24, 37, 57). It is not necessary to include confinement by the nuclear envelope because we are only interested in the loci where phosphorylation occurs, which are 50 kb or less from the DSB. At thermodynamic equilibrium, there is a roughly 0.4 μm RMSD between two loci separated by 50 kb of chromatin (we estimated this based on the persistence length and compaction of the chromosome from Arbona et al. (3) and used the formula for R in the *Supplementary Information, 3D Diffusion Model Derivation*). The nucleus has a diameter of 2 μm, which is much larger than the 0.4 μm RMSD, so loci at 50 kb from the DSB are not confined by the nuclear envelope to stay in closer proximity to the DSB.

Using the equilibrium distribution of worm-like chain conformations is justified because we estimate that loci 50 kb away from each other should encounter each other every few minutes (every few seconds for loci 10 kb away from each other), which is much faster than the few tens-of-minutes time scale over which H2A phosphorylation occurs. We can estimate the contact frequency between two loci because we know the root mean squared distance R at equilibrium for the two loci. We also know the time t for a locus to diffuse a distance equal to R – this is obtained by inspecting the mean squared displacement (MSD) vs. time plot in Hajjoul et al. (5). Counterintuitively, t is equivalent to the time it takes for the two loci to come in contact. This is because chromatin undergoes subdiffusion, and any object moving subdiffusively thoroughly explores its space (6) – i.e. in the time t, the locus thoroughly explores a sphere of radius R. Therefore, loci within a distance R of each other will come in contact during the time t.

Now we introduce the formula for the worm-like chain looping probability. Let *l* be the Kuhn length of the worm-like chain and *x* be the contour length between two particular locations on the chain. $n = x/l$ is therefore the number of Kuhn lengths between the two locations. P_{loop} is the fraction of chain conformations that have these two locations in physical contact. To be considered in physical contact, we say that the 3D distance between the two locations must be less than *g*, where *g* is a small fraction of a Kuhn length (*g* is unitless because it is a fraction). P_{loop} is given by

$$P_{loop}\left(n\right) = 1.34\, g^{3} n^{-3/2} e^{-2n^{-2}} \qquad (11)$$

Note that equation (11) is an approximation – it does not predict P_{loop} exactly. Nevertheless, we compared equation (11) to a simulation of the exact worm-like chain model, and we found that the formula is accurate (i.e. has a maximum error of about 10%) for $g = 0.05$ and $0.7 \le n \le 7$, which are the ranges used when comparing the looping model to the experimental γ-H2AX levels. Equation (11) is based on ref. (7) and is plotted (in a normalized form) in Figure S17. Figure S17 also shows the results of our worm-like chain simulation, which is a Monte Carlo simulation of the worm-like chain model (8) at thermodynamic equilibrium. In our simulation, every Kuhn length is discretized into 1000 small segments. Looping is considered to occur if the two ends of the worm-like chain come less than $g = 0.05$away from each other (i.e. the Kuhn length for *S. cerevisiae* chromatin in units of nanometers is about 180 nm (3), so the interaction distance that we use is about 9 nm).

Now we incorporate the kinase into the model. Suppose the kinase is at the break site, and consider an H2A that is separated from the DSB by *n* Kuhn lengths of chromatin. $P_{loop}\left(n\right)$ is therefore the probability that the chromosome is in a looped conformation in which the kinase and H2A are in physical contact. For H2A phosphorylation to occur, not only is this contact necessary but the kinase must also be in the necessary orientation. Let U be the fraction of orientations that can result in phosphorylation, given that the H2A and kinase are in contact. Let k_{cat} be the rate at which the kinase phosphorylates the H2A, given that the kinase is in contact with the H2A and is in the necessary orientation. Therefore, the rate of phosphorylation of the H2A is

$$k_{phos,\,LM}(n) = k_{cat}\acute{U}P_{loop}(n) \tag{12}$$

where the "LM" subscript stands for the looping model. Substitute equation (11) into equation (12), and replace n with x/l, and we obtain

$$\begin{aligned} k_{phos,\,LM}(x) &= 1.34k_{cat}\acute{U}g^{3}\left(l/x\right)^{3/2} e^{-2(l/x)^{2}} \\ &= \varphi\left(l/x\right)^{3/2} e^{-2(l/x)^{2}} \end{aligned} \tag{13}$$

where $\varphi = 1.34\,k_{cat}\acute{U}g^{3}$. Note that for x and l we use units of kilobase pairs because in our experiments we know the number of kilobase pairs between the DSB and our measured loci.

We construct the model to be consistent with ChIP measurements of Tel1 and Mec1 at the break site, which show their levels increase linearly with time (6, 7). These measurements could indicate two different dynamics. First, they could imply that there is an increasing number of kinases at the break site, and higher numbers of kinases could result in proportionally higher rates of H2A phosphorylation (this model was not considered in the main text). The phosphorylation rate is therefore the product of $k_{phos,\,LM}(x)$ and the number of kinase copies on the DSB. We will refer to this as the "linearly increasing phosphorylation rate."

Alternatively, even with multiple copies of kinases bound near the break site, it is possible that only one or two copies perform phosphorylation. (Hypothetical scenarios that would cause this include these possible examples: there is a row of kinases near the break site, but only the kinase precisely at the DSB is activated, or steric hinderance causes only the kinase copies at the ends of the row to have their active sites accessible to H2As). Thus, in each cell, once a kinase has arrived to the DSB, there is simply a constant rate of H2A phosphorylation given by $k_{phos,\,LM}(x)$ (this model was considered in the main text). We will refer to this as the "constant phosphorylation rate." The constant and linearly increasing phosphorylation rates are the two extremes in possible dynamics; intermediate dynamics could occur – i.e. phosphorylation rates that increase in a sub-linear manner. We only examine the two extremes because they yield the greatest difference in predicted γ-H2AX profiles. We will begin with a derivation that involves the constant phosphorylation rate.

Looping Model with a Constant Phosphorylation Rate

This is the model discussed in the main text.

When a kinase is present on the break site, it phosphorylates H2As at a rate $k_{phos,\,LM}(x)$, so we have

$$\begin{aligned} \frac{dP_{phos}(x,t\,|\,\tau)}{dt} &= \left(1-P_{phos}(x,t\,|\,\tau)\right)k_{phos,\,LM}(x) \\ P_{phos}(x,t\,|\,\tau) &= 0 \text{ for } t<\tau \end{aligned} \tag{14}$$

where $P_{phos}(x,t\,|\,\tau)$ is the probability that the H2A at *x* kilobase pairs from the break site has been phosphorylated by time *t*, given that the kinase arrived to the break site at time *τ*. (The bottom equation of equations (14) states that no phosphorylation takes place until the kinase arrives to the break site). Solving equations (14) gives

$$P_{phos}(x,t\,|\,\tau) = \begin{cases} 1-e^{-k_{phos,\,LM}(x)\,(t-\tau)}, & \text{when } t \ge \tau \\ 0, & \text{when } t < \tau \end{cases} \tag{15}$$

Recall that in the "constant phosphorylation rate" version of the looping model, we only consider a single copy of the kinase at the break site because we assume that additional copies of the kinase would not change the phosphorylation rate. In different cells in the yeast population, the single copy of the kinase arrives to the break site at different times. To take this into account, we perform the same derivation that is in the directed sliding model's section entitled "Derivation that Incorporates the Variability in the Timing of DSB Formation and Arrival of the Kinase to the Break Site:" $P_{phos}(x,t)$, the probability that the H2A at *x* kilobase pairs from the break site has been phosphorylated by time *t*, is given by

$$P_{phos}(x,t) = \int_0^t P_{phos}(x,t\,|\,\tau)PDF(\tau)\,d\tau \tag{16}$$

where $P_{phos}(x,t\,|\,\tau)$ is given by equation (15) and $PDF(\tau)$ is given by equation (8). Note that when using equation (8) for the looping model, k_{init} indicates the rate at which the kinase arrives to the break site (note that this differs from the definition of k_{init} used in the sliding model because in the sliding model k_{init} involves kinase arrival to the break site AND the process of leaving the break site to begin sliding). Upon carrying out the integration in equation (16), we obtain

$$\begin{aligned} P_{phos}(x,t) = 1 &+ \frac{k_{DSB}\,k_{phos,LM}(x)\,e^{-k_{init}t}}{\left(k_{DSB}-k_{init}\right)\left(k_{init}-k_{phos,LM}(x)\right)} \\ &+ \frac{k_{DSB}\,k_{init}e^{-k_{phos,LM}(x)\,t}}{\left(k_{phos,LM}(x)-k_{DSB}\right)\left(k_{init}-k_{phos,LM}(x)\right)} + \frac{k_{init}\,k_{phos,LM}(x)\,e^{-k_{DSB}t}}{\left(k_{init}-k_{DSB}\right)\left(k_{DSB}-k_{phos,LM}(x)\right)} \quad . \end{aligned} \tag{17}$$

Looping Model with a Linearly Increasing Phosphorylation Rate

This model is not included in the main text because the Bayes factor calculations demonstrate that it is worse than the model with the constant phosphorylation rate. In this version of the looping model, the phosphorylation rate is proportional to the number of copies of the kinase that are on the break site. Let $M(t\,|\,\delta)$ be the average number of copies of the kinase on the break site at time *t*, given that the DSB formed at time δ. Therefore, we have

$$\begin{aligned} &\frac{dP_{phos}(x,t\,|\,\delta)}{dt} = M(t\,|\,\delta)\; k_{phos,LM}(x)\;\left(1-P_{phos}(x,t\,|\,\delta)\right) \\ &P_{phos}(x,t\,|\,\delta) = 0 \text{ for } t < \delta \end{aligned} \tag{18}$$

where $P_{phos}(x,t\,|\,\delta)$ is the probability that the H2A at *x* kilobase pairs from the break site has been phosphorylated by time *t*, given that the DSB formed at time δ. (For simplicity, we obtain an approximate solution by using the mean number of kinase copies on the break site $M(t\,|\,\delta)$, ignoring the variance in the numbers of kinase copies.)

The average number of kinase copies at the break site is linear with time (i.e. kinases arrive with a constant rate k_{init}), so $M(t\,|\,\delta) = (t-\delta)k_{init}$. Solving equations (18) using this expression for $M(t\,|\,\delta)$ gives

$$P_{phos}(x,t \mid \delta) = \begin{cases} 1 - e^{-\frac{k_{init} k_{phos,LM}(x)\,(t-\delta)^2}{2}}, & \text{when } t \geq \delta \\ 0, & \text{when } t < \delta \end{cases} \qquad (19)$$

Next we take into account that δ varies across yeast cells in the population. Because the DSB forms at a constant rate k_{DSB}, there is an exponential distribution of waiting times for DSB formation, given by the following probability density function for δ:

$$PDF(\delta) = k_{DSB} e^{-k_{DSB}\delta} \qquad (20)$$

$P_{phos}(x,t)$, the probability that the H2A at *x* kilobase pairs from the break site has been phosphorylated by time *t*, is given by

$$P_{phos}(x,t) = \int_0^t P_{phos}(x,t \mid \delta) PDF(\delta)\, d\delta \qquad (21)$$

We plug equations (19) and (20) into equation (21) and evaluate the integral numerically.

Note that in equation (19), $k_{init}$and $k_{phos,LM}(x)$ never appear separately: they are always multiplied together. Using equation (13), we have $k_{init} k_{phos,LM}(x) = k_{init}\varphi\left(l/x\right)^{3/2} e^{-2(l/x)^2}$, so we define the parameter $\psi = k_{init}\varphi$ (i.e. k_{init} and $\varphi$are not separate parameters in the "Linearly Increasing Phosphorylation Rate" version of the looping model). Therefore, this version of the looping model has only two parameters: ψ, and l.

1D Diffusion Model Simulation

Here we describe additional details of the Gillespie simulations for 1D diffusion that were not discussed in the *Computational Methods* section of the main text. As previously mentioned, we construct all of our models to be consistent with ChIP measurements of Mec1 and Tel1 at the break site, which show Mec1 and Tel1 levels that increase linearly with time. In the 1D diffusion model, linearly increasing kinase levels could be achieved through one of two simple mechanisms, one in which there is a constant rate at which kinases initiate 1D diffusion, and a mechanism in which the rate of diffusion initiation increases linearly with time. The former mechanism is discussed in the main text, while the latter mechanism is not since our Bayes factor calculation demonstrates that the former is more likely to be correct. We will now describe how these mechanisms give rise to linearly increasing kinase levels at the break site and will discuss how these mechanisms are implemented in our simulations.

We begin by describing the mechanism with a constant rate of diffusion initiation. Let $k_{arriveDSB}$ be the rate at which a kinase arrives to the break site and $k_{leaveDSB}$ be the rate at which a kinase leaves the break site to start diffusing along the chromosome. In the mechanism with a constant rate of diffusion initiation, only one kinase copy can leave the break site at a time. (This could happen if the copies of the kinase line up in a row close to the break site, such that the one copy furthest from the DSB is physically blocking the other copies from being able to slide away from the break site). In this scenario, if $k_{arriveDSB} > k_{leaveDSB}$, then copies of the kinase will build up at the break site linearly with time: we will have $M(t) = \left(k_{arriveDSB} - k_{leaveDSB}\right)\left(t - \delta\right)$, where δ is the time when the DSB forms, and $M(t)$ is the average number of kinases on the break site $\left(t - \delta\right)$ minutes after the formation of the DSB.

We perform this simulation by having a single rate-limiting step described by the rate k_{init}, where k_{init} is the rate at which a kinase copy arrives to the break site and then departs the break site to diffuse along the chromosome. (Note that it is only necessary to use this single rate rather than the two rates $k_{arriveDSB}$ and $k_{leaveDSB}$: using the single rate becomes equivalent to using two rates if $k_{arriveDSB}$ is fast. If $k_{arriveDSB}$ is slow, then the situation becomes equivalent to the mechanism in which the rate of diffusion initiation increases linearly with time, which is discussed in the next paragraph.) Throughout the entire duration of the simulation, kinase copies continue to start at rate k_{init}. Therefore, in our simulations there can be many kinase copies diffusing concurrently on the chromosome.

In the mechanism in which the rate of diffusion initiation increases linearly with time, the kinases do not block each other, but rather all kinases on the break site are capable of sliding away from the break site. In this case, the number of kinases that leave the break site per unit time is $M(t)\, k_{leaveDSB}$. If $k_{arriveDSB} >> M(t) k_{leaveDSB}$, then copies of the kinase will build up at the break site linearly with time: we will have $M(t) = k_{arriveDSB}(t-\delta)$. The number of kinases that leave the break site per unit time will therefore be $k_{leaveDSB}k_{arriveDSB}(t-\delta)$. In other words, unlike in the first mechanism where there is a constant rate of kinase copies starting to diffuse along the chromosome, in this mechanism the rate of kinase copies starting to diffuse grows linearly with time. We implement this mechanism's simulation by having each kinase copy arrive to the break site at a rate $k_{arriveDSB}$ and leave the break site at a rate $k_{leaveDSB}$. Note, however, that these rates are not separate parameters because the dynamics are governed by the product $k_{leaveDSB}k_{arriveDSB}$, so when we vary parameter sets, we only vary $k_{arriveDSB}$, and we simply set $k_{leaveDSB} = 0.0005/\text{minute}$ (we chose this value since it is slow enough for there to be linear growth in the number of kinases at the break site over several hours). When we report parameter values, we report z, where $z = k_{leaveDSB}k_{arriveDSB}$. Kinase copies begin diffusing throughout the entire duration of the simulation, so there can be many kinase copies diffusing concurrently on the chromosome. For simplicity, in all 1D diffusion simulations we assume the kinases do not interact with each other (i.e. no traffic jams); to avoid the regime where traffic jams would become likely, we limit how large k_{init} and z can be in order to limit the total number of kinases along the chromosome.

3D Diffusion Model Derivation

We treat the kinase as a randomly diffusing particle and each H2A histone as a spherical target of radius a. Given infinite time, a particle diffusing without constraints can either hit the target or diffuse infinitely far away without ever hitting the target – the probability that the particle hits the target is $P_{contact} = a/R$ (11), where R is the 3D distance between the target and particle at the beginning of the particle's trajectory (Figure S18). The infinite time assumption approximates our situation because the hour time scale of phosphorylation is much longer than the seconds time scale presumably required for proteins to diffuse across the nucleus (see ref. (12) for diffusion in the nucleus of human cells). The assumption of no constraints can be applied to our system despite the presence of the nuclear envelope. Confinement by the nuclear membrane keeps the kinases in the nucleus, so the kinases will traverse the nucleus many times, presumably continuing to phosphorylate H2As, which results in a background γ-H2AX signal that is approximately the same for all H2As. It is a reasonable assumption that the kinase's catalytic rate is slow enough that over the time scale of the experiment, the kinases would only have time to phosphorylate a small fraction of the H2As throughout the nucleus. The background signal would therefore be minimal and can be ignored, allowing us to simply have $P_{contact} = a/R$. (Alternatively, it is also possible that the background signal is not negligible, but having a significant background signal would make the 3D diffusion model not match the experimental γ-H2AX profiles, so we do not consider this scenario). In summary, the H2As near the break site are likely to be contacted by the kinases as the kinases diffuse outward from the break site, so H2As near the break are likely to be phosphorylated; H2As far from the break only have a very small probability of phosphorylation because only a small fraction of all the H2As in the nucleus will be phosphorylated as a result of the slow catalytic rate.

The kinase starts its trajectory at the break site, and the target is an H2A located x kb from the DSB. The distance R is taken to be the root mean squared distance from the H2A to the DSB, given by a worm-like chain treatment of the chromatin at thermodynamic equilibrium: $R = \frac{l}{\eta}\sqrt{\frac{e^{-2x/l} + 2x/l - 1}{2}}$, where l is the chromatin's Kuhn length, and η is the chromatin compaction, the number of kilobases of DNA per nanometer of chromatin fiber (13). Therefore, $P_{contact}(x,l) = \frac{\sqrt{2}a\eta}{l\sqrt{e^{-2x/l} + 2x/l - 1}}$. According to $P_{contact}$, H2As further from the DSB are less likely to be contacted by the kinase.

We assume many copies of the kinase come on and off the DSB, where the rate of leaving the DSB is $k_{leaveDSB}$. Therefore, an H2A located x kb from the DSB is hit by kinases at a rate $P_{contact}\left(x,l\right)k_{leaveDSB}$. If υ is the fraction of contacts that results in phosphorylation, the rate at which the H2A is phosphorylated is $k_{phos,3DDM}(x) = \upsilon P_{contact}\left(x,l\right)k_{leaveDSB}$ (the subscript "3DDM" stands for the 3D diffusion model). Plugging in the expression for $P_{contact}$, we have

$$k_{phos,3DDM}(x) = \frac{\omega}{\sqrt{e^{-2x/l} + 2x/l - 1}} \tag{22}$$

where $\omega = \frac{\sqrt{2}\upsilon a\eta}{l} k_{leaveDSB}$.

There are two versions of the 3D diffusion model: one with a constant rate of diffusion initiation (which is the model discussed in the main text), and a version with a linearly increasing rate of diffusion initiation. The rationale for trying these two model variants is the same as that described in the *1D Diffusion Model Simulation* section above. The Bayes factor analysis determined that the 3D diffusion model with the constant rate is more likely to be correct than the 3D diffusion model with the linearly increasing rate.

The 3D diffusion model with a constant rate of diffusion initiation involves kinases leaving the break site at a constant rate and therefore phosphorylating H2As at a constant rate. This model is derived in exactly the same way as the looping model with a constant phosphorylation rate (equation (17)), except the phosphorylation rate $k_{phos,\,LM}(x)$ is replaced by $k_{phos,\,3DDM}(x)$, so we obtain

$$\begin{aligned} P_{phos}(x,t) = 1 &+ \frac{k_{DSB}k_{phos,\,3DDM}(x)\; e^{-k_{init}t}}{\left(k_{DSB}-k_{init}\right)\left(k_{init}-k_{phos,\,3DDM}(x)\right)} \\ &+ \frac{k_{init}k_{phos,\,3DDM}(x)\, e^{-k_{DSB}t}}{\left(k_{init}-k_{DSB}\right)\left(k_{DSB}-k_{phos,\,3DDM}(x)\right)} \\ &+ \frac{k_{DSB}k_{init}e^{-k_{phos,\,3DDM}(x)\,t}}{\left(k_{phos,\,3DDM}(x)-k_{DSB}\right)\left(k_{init}-k_{phos,\,3DDM}(x)\right)} \end{aligned} \tag{23}$$

The 3D diffusion model with a linearly increasing rate of diffusion initiation involves kinases leaving the break site at an increasing rate. This model is derived in exactly the same way as the looping model with a linearly increasing phosphorylation rate (equations (19)-(21)), except the phosphorylation rate $k_{phos,\,LM}(x)$ is replaced by $k_{phos,\,3DDM}(x)$, so we have the following equations:

$$
\begin{aligned}
&P_{phos}(x,t\mid\delta)=\begin{cases}1-e^{-\frac{k_{init}k_{phos,3DDM}(x)\,(t-\delta)^2}{2}}, & \text{when } t\geq\delta\\ 0, & \text{when } t<\delta\end{cases}\\
&PDF(\delta)=k_{DSB}e^{-k_{DSB}\delta} \qquad\qquad (24)\\
&P_{phos}(x,t)=\int_0^t P_{phos}(x,t\mid\delta)PDF(\delta)\,d\delta
\end{aligned}
$$

where the integral is evaluated numerically. k_{init} and $k_{phos,3DDM}$ always appear multiplied together. From equation (22), we see that $k_{init}k_{phos,3DDM}(x)=\dfrac{k_{init}\,\omega}{\sqrt{e^{-2x/l}+2x/l-1}}$, so we define the parameter $\zeta=k_{init}\,\omega$. Therefore, this version of the 3D diffusion model has only two parameters: ζ, and l.

Accounting for γ-H2AX Measurements near the Recombination Enhancer

When predicting γ-H2AX levels near the Recombination Enhancer (RE), we take into account the protein-mediated binding of RE to the break site at the MAT locus (14, 15). With RE bound to the DSB, RE-adjacent loci (that are 5 or 10 kb from RE) are now in close spatial proximity to the DSB, so the 3D models predict that the kinases can reach the RE-adjacent sites. 1D models predict that the kinases cannot reach RE-adjacent sites because RE is located 171 kb away from MAT. For 3D models, we include two additional parameters in order to take into account the binding of RE to MAT. Initially there is a period when RE is not bound to the DSB at all, but with rate k_{RE} (k_{RE} may represent the rate at which proteins at MAT undergo phosphorylation at their threonine residues that are necessary to mediate the RE-MAT interaction) the cell transitions to the state in which RE and the DSB are bound some fraction of the time (denoted by F_{RE}), at which point the kinase can phosphorylate RE-adjacent sites. The rate of phosphorylation for an H2A that is *x* kb from RE is assumed to equal the phosphorylation rate for an H2A that is *x* kb from the DSB multiplied by F_{RE}. In other words, for the RE-adjacent sites, $P_{contact}(x,l)$ in the 3D diffusion model and $P_{loop}(x,l)$ in the looping model are multiplied by F_{RE} because the kinase only comes in contact with the RE-adjacent sites during the fraction of the time when RE and MAT are bound.

Some Models Require Kinase Activation at the DSB

The 3D diffusion, 1D diffusion and directed sliding models require that the kinase becomes activated upon arrival to the break site. Without this activation, these models would not predict preferential phosphorylation of H2As close to the break site; the kinase becomes activated at the DSB and is more likely to encounter closer H2As than farther H2As. To further argue this point, consider a model in which the kinase is activated without having to encounter the DSB. At the moment when the DSB is formed, the kinase is at some arbitrary location in the nucleus, so it is equally likely to diffuse to any genetic locus and then start phosphorylating H2As from that locus (this applies for directed sliding, 1D diffusion and 3D diffusion). Simply assuming strong binding between the kinase and the break site would not result in increased phosphorylation near the DSB. Strong binding to the DSB would merely hold the kinase in place for a while – i.e. kinases that happen to come in contact with the DSB would end up wasting their time sitting on the DSB, so they would have less time to phosphorylate H2As. As previously noted, a precedent for kinase activation was found by an *in vivo* study of ATM, the mammalian homolog of Tel1: upon binding to the MRN complex at the break site, ATM undergoes autophosphorylation and thus becomes active (16).

Note that the 1D diffusion and directed sliding models are mathematically equivalent to models in which many copies of the kinase bind along the chromatin, each binding to the next adjacent H2A. In this case, kinase activation could take place but is not required in the model. This is because the strong binding of the kinase to the break site could serve to nucleate the formation of the row of kinases. The directed sliding model is also equivalent to a model in which the kinase remains bound to the break site while the nearby chromatin slides past it – e.g. this would happen if the cohesin complex binds to the DSB and extrudes chromatin through the cohesin ring, causing the DSB-bound kinase to slide past the nearby chromatin; such a model does not require kinase activation at the break site (recent work in mammalian cells suggests that such an extrusion mechanism may be responsible for the formation of a γ-H2AX region around a DSB (17)).

Also note that the looping model does not require activation at the DSB: H2As are preferentially phosphorylated in the vicinity of the DSB because the kinase binds the DSB and the looping of the chromosome brings the kinase into contact with nearby H2As.

A quantitative model of ChIP

In order to quantitatively compare our phosphorylation propagation models to ChIP data, we must have a quantitative understanding of ChIP. It is not sufficient to merely have the qualitative understanding that a higher ChIP signal indicates the presence of more γ-H2AXs. Our phosphorylation propagation models predict the probability $P_{phos}(x,t)$ that an H2A has been phosphorylated, where *x* is the number of kilobase pairs separating the H2A from the break site, and *t* is the elapsed time since the addition of galactose (galactose induces production of HO-endonuclease, the enzyme that forms the DSB). Measuring the ChIP signal does not directly give us the probability of phosphorylation. Rather, the ChIP signal is some function of this probability: the function $S(P_{phos})$ will represent the ChIP signal. Below, we make a model of the ChIP process in order to derive the functional form of S. Having obtained the functional form of *S*, we can use it in conjunction with the $P_{phos}(x,t)$ predicted by each phosphorylation propagation mechanism: We plug in the predicted $P_{phos}(x,t)$ as the argument of *S* to yield the predicted γ-H2AX ChIP profile $S(P_{phos}(x,t))$ for each mechanism of phosphorylation propagation. We can then compare each mechanism's predicted γ-H2AX ChIP profile to the experimentally-measured ChIP profile.

The experimental ChIP signal that we report is $S = 280\,\dfrac{\gamma H2AX \quad signal}{control \quad signal}$. *γ-H2AX signal* is the qPCR signal for the DNA that has γ-H2AX bound to it; *control signal* is the qPCR signal from all DNA at the same locus (i.e. all DNA regardless of whether it has γ-H2AX on it). The 280 is present because the sample for the control was diluted by a factor of 280 relative to the sample for the *γ-H2AX signal*. We quantitatively model *S* by taking into account that only some of the DNA with γ-H2AX on it is pulled down by antibodies during ChIP: let $P_{pull-down}(P_{phos})$ be the probability of pulling down DNA at the measured locus, which depends on the P_{phos} at that locus (discussed further below). We also take into account that aside from the pull-down, other steps (e.g. washing steps) in ChIP may reduce the recovery of DNA. Let *C* be 280 multiplied the probability that the

DNA will be recovered in all the other steps, given that it was pulled down by the antibodies. Therefore, our model for the ChIP signal is $S(P_{phos}) = CP_{pull-down}(P_{phos})$.

Let us now quantitatively model $P_{pull-down}$. In the ChIP protocol, sonication results in DNA fragments roughly 500 bp in length, containing multiple H2As. The DNA fragment comes to the surface or interior of a porous agarose bead, where the DNA fragment's γ-H2AXs can bind to antibodies that are attached to the bead. We make two assumptions: (1) The binding of a single antibody to a single γ -H2AX results in the DNA fragment being pulled down. (Even if there are multiple γ-H2AXs on a DNA fragment, only one γ-H2AX needs to be bound by an antibody for the DNA fragment to be pulled down). Let the parameter *f* be the probability that a particular γ -H2AX is bound by an antibody. (2) The second assumption is that the antibodies bind independently of each other – i.e. an antibody binding to one γ-H2AX has no effect on whether an antibody binds to another γ-H2AX on the same DNA fragment.

These two assumptions are captured mathematically in the following manner: Let N_{H2A} be the average number of phosphorylatable H2A's on a DNA fragment – e.g. $N_{H2A} = 6$ in cells with all wild-type H2As, and we use $N_{H2A} = 3$ in cells with only 1/2 wild-type H2As. $N_{H2A}P_{phos}$ is the average number of γ-H2AXs on a DNA fragment. The probability that the DNA fragment is pulled down is $P_{pull-down} = 1-(1-f)^{N_{H2A}P_{phos}}$ because this is the probability that at least one γ-H2AX is successfully bound by an antibody (i.e. it is 1 minus the probability that none of the γ-H2AXs are bound by antibodies). This expression is not valid for $N_{H2A}P_{phos} < 1$ (i.e. if the average number of γ-H2AXs on a DNA fragment is less than 1). If $N_{H2A}P_{phos} < 1$, then we use the expression $P_{pull-down} = N_{H2A}P_{phos}f$ because $N_{H2A}P_{phos}$ is the probability of one γ-H2AX being present on the DNA fragment, and *f* is the probability that the DNA fragment is pulled down given that there is one γ-H2AX on the fragment. Therefore, our quantitative model of the ChIP signal is the following:

$$S(P_{phos}) = \begin{cases} C\left(1-(1-f)^{N_{H2A}P_{phos}}\right), & \text{when } N_{H2A}P_{phos} \geq 1 \\ CN_{H2A}P_{phos}f, & \text{when } N_{H2A}P_{phos} < 1 \end{cases} \tag{25}$$

where N_{H2A}, f and C are parameters of the quantitative ChIP model, and P_{phos} includes both the predicted DSB-dependent phosphorylation and the basal phosphorylation that occurs prior to DSB formation (see the next section on basal γ-H2AX levels). Equations (25) are applicable to all models besides the directed sliding model, which is discussed below in *A quantitative model of ChIP for the directed sliding model*.

As an example of the predictions from this model of ChIP, suppose it were the case that all the phosphorylatable H2As at a locus were phosphorylated – i.e. $P_{phos}(x,t) = 1$. We use $f = 0.16$ and $N_{H2A} = 6$ for the wild type and $N_{H2A} = 3$ for the mutant strain, which are the best parameter values extracted from Bayesian parameter estimation (as shown in Table 3). Then although the mutant strain has only 1/2 as many γ -H2AXs as the wild type, the mutant strain will have a ChIP signal that is 0.63 times the signal of the wild-type strain.

In the looping and 3D diffusion models, phosphorylation of one H2A is independent of phosphorylation of another H2A, even in the case of H2As on the same DNA fragment. For the looping model, this is because phosphorylation occurs according to the thermodynamic equilibrium looping probabilities, so the phosphorylation of one H2A has no influence on whether a nearby H2A is phosphorylated. For the 3D diffusion model, a single copy of a kinase is unlikely to contact more than one H2A on a given DNA fragment since the probability of the kinase contacting an H2A is at most 0.1 (this is estimated by plugging in reasonable values for the coefficients in the formula for $P_{contact}(x,l)$ in the *Supplementary Information, 3D Diffusion Model Derivation*); therefore, the phosphorylation of H2As is effectively uncorrelated. The independence of H2A phosphorylation means that the number of γ-H2AXs on a DNA fragment is binomially distributed with a peak at $N_{H2A}P_{phos}$. In the looping and 3D diffusion models, for simplicity we ignore the spread of the binomial distribution and just use $N_{H2A}P_{phos}$ as the number of γ-H2AXs on a DNA fragment. This simplifying assumption is what we included in equations (25).

In the 1D diffusion model, however, phosphorylation of one H2A is not independent of another

H2A on the same DNA fragment, and so it is possible that there would be a wide range in the number of γ-H2AXs on a DNA fragment, and so using just the mean number may not be accurate. Therefore, in every run of the 1D diffusion simulation, we record the number of γ-H2AXs on each DNA fragment. We apply the ChIP model to every DNA fragment and then take the average over the fragments from all runs in order to get the net ChIP signal.

Basal γ-H2AX levels are incorporated into the predicted ChIP signals

Experimentally we measure a basal level of γ-H2AX on the chromosome that exists at time 0 (which is before the DSB forms) – this is the ChIP signal measured at time 0 in Figures 1, 2, 4, 5, 6 and S3. We use the mean values of the basal γ-H2AX profile to serve as the initial ChIP signal in every model of γ-H2AX spreading (rather than starting from a ChIP signal of 0). Because basal phosphorylation and DSB-dependent phosphorylation are presumably independent of each other, the probability of phosphorylation as a result of either basal or DSB-dependent phosphorylation is

$$P_{phos,\,total}(x,t) = P_{phos,\,basal}(x) + \left(1 - P_{phos,\,basal}(x)\right) P_{phos}(x,t) \qquad (26)$$

where $P_{phos}(x,t)$ is the DSB-dependent phosphorylation derived for the model of γ-H2AX spreading. To obtain $P_{phos,\,basal}$, we note that the basal ChIP signals are small, so $P_{phos,\,basal}$ must be small. Therefore, we can use the bottom equation (25), and rearrange to get $P_{phos,\,basal}(x) = \dfrac{S_{exp\,basal}(x)}{CN_{H2A}f}$, where $S_{exp\,basal}(x)$ is the experimentally measured basal ChIP signal. To obtain the predicted ChIP signals, $P_{phos,\,total}(x,t)$ is what we actually use in equations (25) in place of P_{phos}.

A quantitative model of ChIP for the directed sliding model

For the directed sliding model, we modify equations (25). In the directed sliding model we assume that whenever a kinase slides to a locus, it phosphorylates all H2As there. However, the kinase does not make it all the way to every locus. In the directed sliding model, $P_{phos}(x,t)$ is equivalent to the probability that the kinase arrives to location *x*. If the kinase does not arrive to the location *x*, then the ChIP signal is the basal ChIP signal $S_{exp\,basal}(x)$, but if the kinase does arrive to the location, then the ChIP signal is $C\left(1-(1-f)^{N_{H2A}}\right)$. Therefore, the ChIP signal for the directed sliding model is given by

$$S(P_{phos}) = S_{exp\,basal}(x)\left(1-P_{phos}(x,t)\right) + P_{phos}(x,t)\,C\left(1-(1-f)^{N_{H2A}}\right) \tag{27}$$

Bayes factor calculation

The Bayes factor is given by the ratio of marginal likelihoods for two models, Models A and B:

$$\text{Bayes Factor} = \frac{\int P(\vec{y}\,|\,\vec{\theta}_A, \text{Model A})\,P(\vec{\theta}_A)\,d\vec{\theta}_A}{\int P(\vec{y}\,|\,\vec{\theta}_B, \text{Model B})\,P(\vec{\theta}_B)\,d\vec{\theta}_B} \tag{28}$$

where $P(\vec{y}\,|\,\vec{\theta}_A, \text{Model A})$ is the likelihood of the experimental data $\vec{y}$ given Model A and the model parameters $\vec{\theta}_A$, and $P(\vec{\theta}_A)$ is the prior probability of $\vec{\theta}_A$(likewise for Model B). These are discussed below. In the tables displaying the Bayes factors (Table 1, 2 and S1), Model B is always the model with the highest marginal likelihood compared to the other models in the table.

We use previous studies to estimate the range of possible parameter values – the integral in equation (28) is over this range. The previous studies measured the chromatin Kuhn length (95% CI is 8.4-15 kb) and linear density of chromatin DNA (95% CI is 56-68 bp/nm) (3)(48–50), and density of the nucleosomes along the chromatin (about 170 bp/nucleosome) (18) and provided data on the kinetics of *in vivo* H2A phosphorylation that allow us to constrain kinetic parameter ranges (19). Ref. (14) was used to constrain RE parameters. In some cases, there is some arbitrariness in the choice of the range, but choosing a different range (that is still reasonable given the previous studies) only changes the Bayes factors by an order of magnitude. The ChIP parameter ranges are as follows: *f* is allowed to vary between 0 and 1, *N* is allowed to be 2, 4 or 6 H2As, and *C* is allowed to vary between 8.3 and 280, which is based on our measurements of DNA recovery from ChIP compared to samples in which PCR was performed without ChIP.

The functional form of the prior probability distribution $P(\theta)$ for each parameter θ is as follows: For the parameters whose values we know within an order of magnitude (i.e. the Kuhn length l

and ChIP parameter N_{H2A}), we use the uniform prior $P(\theta) = \text{constant}$. For parameters that are less certain, we use Jeffreys priors. However, it is difficult to obtain exact Jeffreys priors given the complexity of our models' functional forms, so we use Jeffreys priors from similar but simpler scenarios. For parameters that represent the probability of a binary event (i.e. the ChIP parameter f, the directed sliding model's parameter q, and the RE-MAT binding fraction F_{RE}), $P(\theta) = \frac{1}{\sqrt{\theta(1-\theta)}}$. All other parameters are assigned prior distributions of $P(\theta) = \frac{1}{\theta}$, which is the Jeffreys prior for the rate parameter of an exponential distribution (17). All prior distributions are normalized and constrained to be within the estimated range of possible values (i.e. $P(\theta) = 0$ if θ is outside the range of possible values). For simplicity, we assume that $P(\vec{\theta})$ for the parameter set $\vec{\theta}$ is the product of the priors $\prod_i P(\theta_i)$ for the individual parameters θ_i.

Because our priors are not precisely Jeffreys priors, let us estimate the extent to which this lack of precision could affect the Bayes factor. To do so, one can calculate the Bayes factor using a different prior. For example, consider using a uniform prior for all model parameters for both the directed sliding model and the 1D diffusion model. For most of the parameters, a uniform prior is quite different from the Jeffreys prior; the uniform prior will serve as an extreme example, so the Bayes factor will presumably be changed by more than it would be if we were able to use the exact Jeffreys prior. As shown in Table 2 of the main text, the Bayes factor is 10^{-6} when Mec1 is undergoing 3D diffusion and Tel1 is undergoing 1D diffusion (this Bayes factor is in comparison to Mec1 3D diffusion with Tel1 directed sliding). Using all uniform priors, this Bayes factor becomes 10^{-7}. Therefore, using a prior with a very different functional form can change the Bayes factor by an order of magnitude but does not change our conclusions.

Finally, we discuss the likelihood function. Consider a particular theory, e.g. Model A. For a particular parameter set $\vec{\theta}$ and for the *i*th measurement condition (each measurement condition is composed of the yeast strain, the time point and the location on the chromosome), Model A predicts a single γ-H2AX ChIP signal S_i. However, because there is measurement error in the experiments, our theory should predict that the experimental data will have some spread about the mean predicted ChIP signal. Therefore, we incorporate an error model into the theory, which we assume to be Gaussian error – i.e. model A predicts that the mean ChIP signal is S_i and predicts a Gaussian spread about the mean with standard deviation σ_i. Hence the likelihood function is

$$P(\vec{y} \mid \vec{\theta}_A, \text{Model A}) = \prod_{i,j} \left[\frac{1}{\sqrt{2\pi}\,\sigma_i} \exp\left(\frac{-(S_i - y_{ij})^2}{2\sigma_i^2} \right) \right] \tag{29}$$

The experimentally measured ChIP signal y_{ij} has the subscript *i* for the measurement condition and the subscript *j* because there are multiple data collected for the same measurement condition.

Analysis of all of our ChIP data revealed that for each measurement condition, the standard deviation of the ChIP data is approximately equal to the mean ChIP signal multiplied by 0.35. Therefore, our error model can use $\sigma_i = 0.35 S_i$. Including this into equation (29) yields

$$P(\vec{y} \mid \vec{\theta}_A, \text{Model A}) = \prod_{i,j} \left[\frac{1}{0.35\sqrt{2\pi}\,S_i} \exp\left(\frac{-(S_i - y_{ij})^2}{2(0.35\,S_i)^2} \right) \right] \tag{30}$$

Finally, the integral in equation (28) is carried out by evaluating the integrand at points on a grid in parameter space and then using a Riemann sum.

As previously discussed, most theories have two variants: (1) a model in which there is an increasing phosphorylation rate or increasing rate of diffusion initiation, and (2) a model in which there is a constant phosphorylation rate or constant rate of diffusion initiation. For each theory, we use the best variant when reporting the Bayes factors. (We found that the constant phosphorylation rate/constant diffusion initiation rate models always fit the data better than the models with the increasing rates).

When calculating the Bayes factor for Tel1 and Mec1 models simultaneously, we exclude the Tel1 3D models because they were proven to be very unlikely from the Bayes factor analysis of Tel1 individually. This exclusion is justified because the analysis in Table 1 indicates that the 1D models are extremely favored for Tel1, and by inspecting the best ChIP parameter values for the various Tel1 models, we see that the 1D models would still be the best models for Tel1 even when constrained to have the same ChIP parameter values as Mec1.

Supplemental Figures

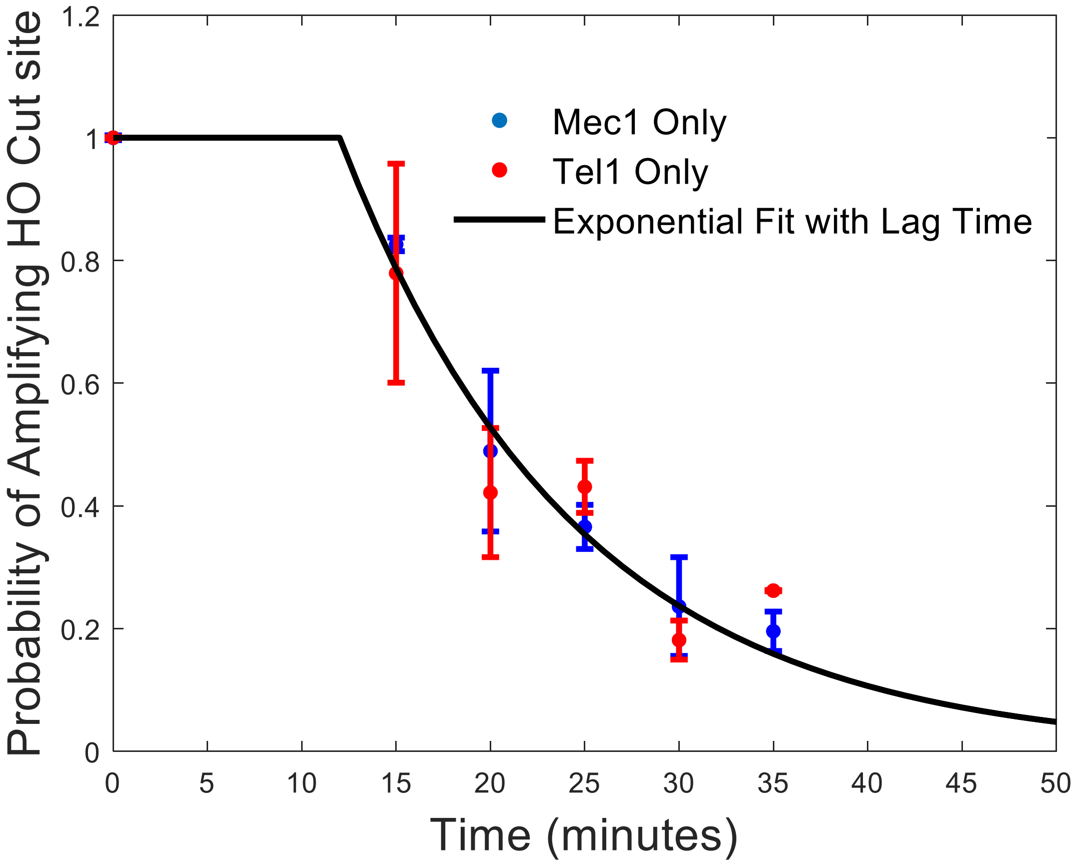

Figure S1: Kinetics of DSB induction

The amount of cleavage at the MAT locus by HO endonuclease after galactose induction was monitored in strains deleted for *YKU80* and carrying either Mec1 (blue) or Tel1 (red). qPCR was performed with primers flanking the cut site to quantify the levels of cleavage over 35 mins. In the presence of a DSB, qPCR fails to amplify the DNA. Approximately, 80% cutting was achieved by 30 mins. The black line is an exponential fit to both strains, using a lag time of 12 minutes (reflecting transcription and translation of the HO endonuclease) and a DNA cleavage rate of k_{DSB} = 0.08/minute. The lag time and k_{DSB} are used in calculating our models of γ-H2AX spreading. Error bars represent the standard error of the mean from n≥3 measurements.

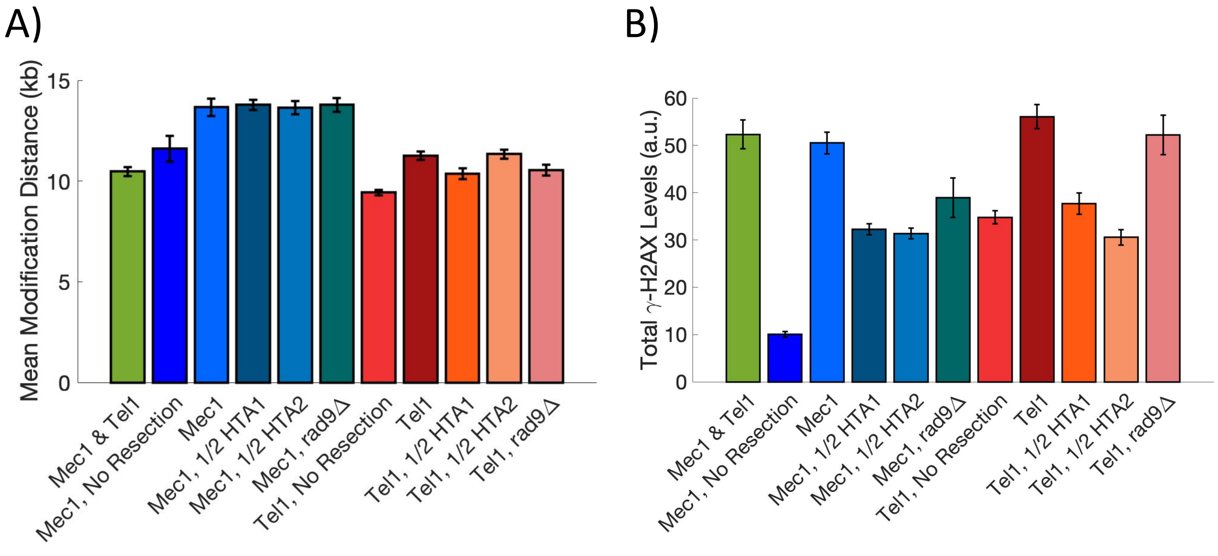

Figure S2: Mean modification distance and total γ-H2AX accumulation

A) The mean modification distance (MMD), the distance from the break that encompasses half the γ-H2AX profile, is displayed for all strains at 75 min except for Mec1, Ddc2 O/E which was measured at 60 min. Error bars represent the standard error of the mean. **B)** Total γ-H2AX levels were calculated by summing up γ-H2AX levels across all measured distances at 75 min. Error bars represent the standard error of the mean.

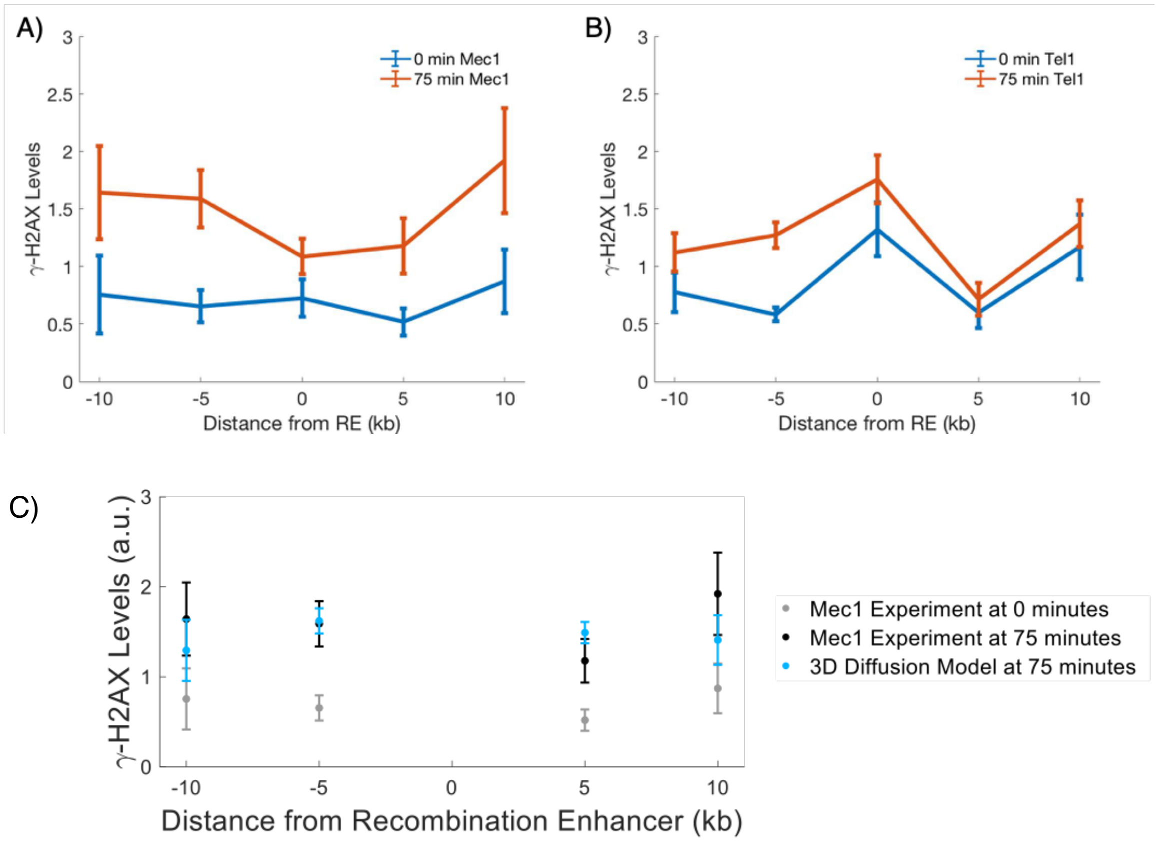

Figure S3: γ-H2AX measurements around RE

γ-H2AX levels measured around the recombination enhancer (RE), a locus on ChrIII known to interact with the MAT locus by forming a chromatin loop. **A)** γ-H2AX formation around RE by Mec1. Error bars represent standard error of the mean from n≥3 measurements. **B)** γ-H2AX formation around RE by Tel1. Error bars represent standard error of the mean from n≥3 measurements. **C)** Comparison of theoretical predictions from 3D diffusion (blue) with experimentally measured γ-H2AX profile around RE by Mec1. The experimental data at 0 min and 75 mins are shown in grey and black, respectively. Experimental error bars are the standard error of the mean from n≥3 measurements. Theoretical predictions from 3D diffusion were generated using the parameters listed in Table 3 with the exception of k_{init} = 0.025/minute, to account for an initial delay is RE binding and RE-DSB interaction which occurs 19% of the time (2). The data point at RE was excluded from the plot since theoretical model does not make predictions at this point. The experimentally measured background was also used as the background for the theoretical curves.

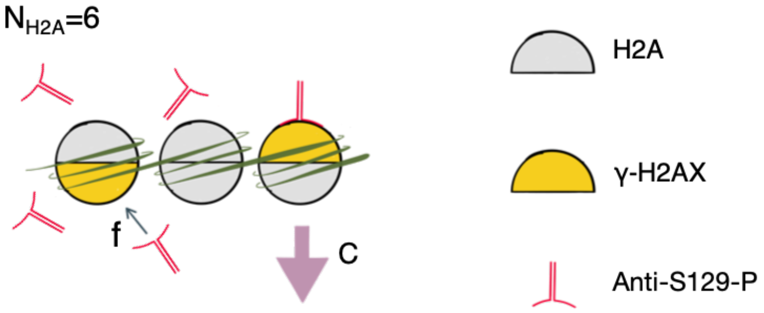

Figure S4: Chromatin fragment recovery

Sonication during ChIP yields chromatin of ~500bp. The parameter N_{H2A} describes the average number of H2As (grey) present on the DNA fragment. In this depiction, N_{H2A}=6. γ-H2AX (yellow) is bound by antibodies (red) with probability *f*. Antibody binding to one γ-H2AX is independent of the other H2A sites on the same chromatin fragment. The binding of one antibody is sufficient for the pull down of the entire fragment (purple arrow). The recovery of the fragment is multiplied by the parameter *C* to account for the loss of DNA during the wash steps in ChIP.

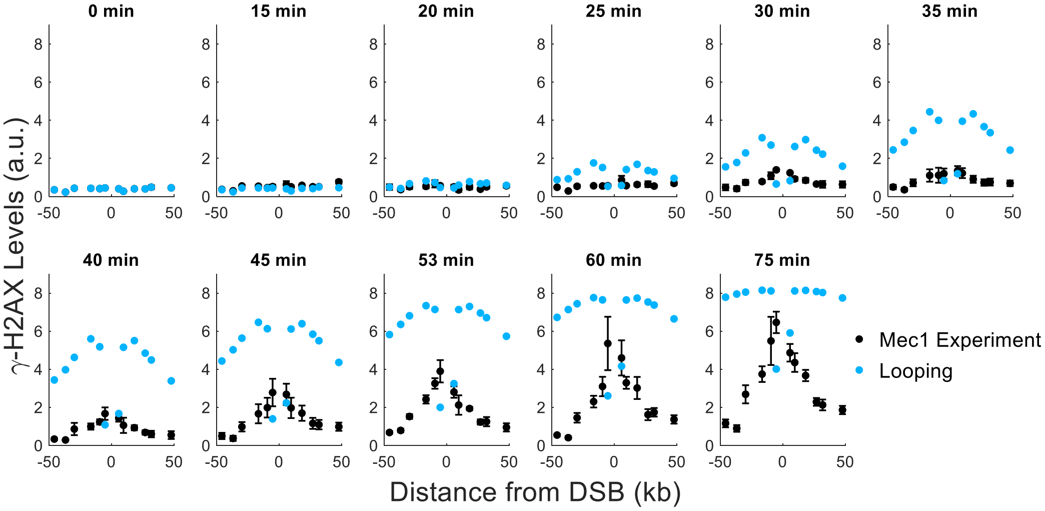

Figure S5: Comparison of experimental data by Mec1 to a looping model with a linearly increasing phosphorylation rate. This model fits the data much worse than the best model, which is shown in Figure 4. Experimental error bars are the standard error of the mean from n≥3 measurements. Bayesian parameter estimation was used to simultaneously fit the model to the data shown here and to the RE-adjacent measurements from Figure S3. The optimal parameter values from Bayesian parameter estimation were used to plot the model, and are as follows: $C = 44$, $f = 0.035$, $N_{H2A} = 6$, $l = 8.4$ kb, and $\psi = 0.039/\text{minute}^2$. To cut down on computation time, all plots in the *Supplementary Information* were fit separately for the Mec1 data and Tel1 data – i.e. Mec1 and Tel1 were not assumed to share the same values of any parameters because it is too computationally expensive to perform a simultaneous calculation for all pairs of Mec1 and Tel1 models. (In Figure 4 and Table 2, however, we impose the constraint that Mec1 and Tel1 have the same values of the ChIP parameters C, f and N_{H2A}).

The exceptionally poor fit of the looping model to the data stems from the constraint that the Kuhn length is at least 8.4 kb, as determined by Arbona et al. (3). With a Kuhn length of at least 8.4 kb, the worm-like chain model predicts that the looping probability is very small for sites closer than 8.4 kb from the break end. However, our data shows that most of the phosphorylation occurs at these closer sites. Therefore, to accommodate this discrepancy, the best fit is achieved via a high catalytic rate for the kinases. (In the looping model, the catalytic rate is part of the parameter φ). The high k_{cat} makes the looping model predict that the loci within 8.4 kb from the break will be phosphorylated almost at levels seen in our experiments, but also predicts the more distant loci will be phosphorylated at even higher levels such that they become saturated and parts of the curve becomes flat. Due to the constraints on the Kuhn length, it is not possible to achieve a good fit to both the close and distant loci.

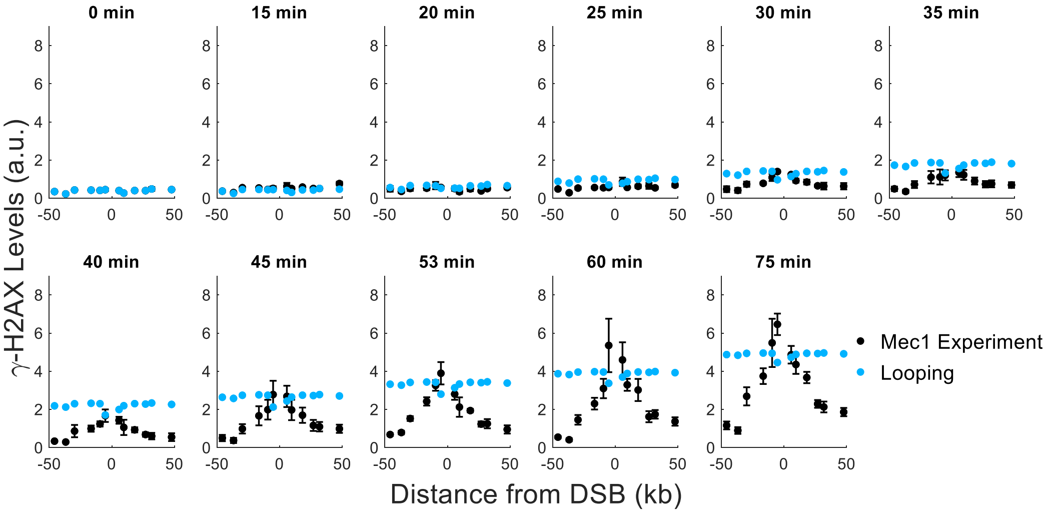

Figure S6: Comparison of experimental data by Mec1 to a looping model with a constant phosphorylation rate. The best model parameters are C = 120, f = 0.035, N_{H2A} = 2, l = 8.4 kb, φ = 11/minute, and k_{init} = 0.017/minute. The catalytic rate in the looping model (which is part of φ) is high, causing the H2As to become saturated. The flat profile increases over time as more of the cells in the population have kinases arrive to the break site. For further details and a discussion of the poor fit of the theory to the data, refer to the caption of Figure S5.

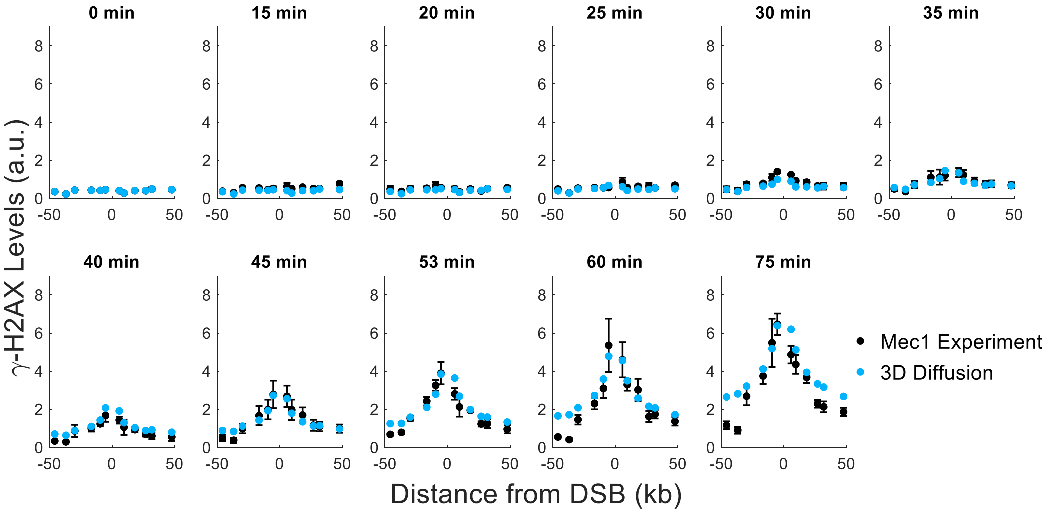

Figure S7: Comparison of experimental data by Mec1 to a 3D diffusion model with a linearly increasing rate of diffusion initiation. The best model parameters are $C = 13$, $f = 0.16$, $N_{H2A} = 6$, $l = 15$ kb, and $\zeta = 3.7\times10^{-4}$/minute^2. For further details, refer to the caption of Figure S5.

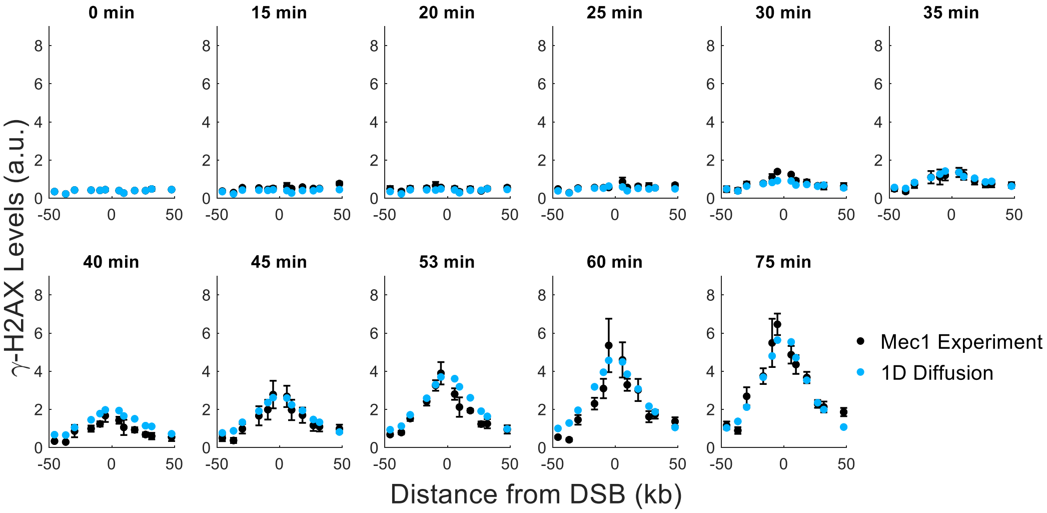

Figure S8: Comparison of experimental data by Mec1 to a 1D diffusion model with a linearly increasing rate of diffusion initiation. The best model parameters are $C = 11$, $f = 0.80$, $N_{H2A} = 6$, $D = 18$ kb^2/minute, $k_{cat} = 0.039$/minute, and $z = 84$/minute^2. For further details, refer to the caption of Figure S5.

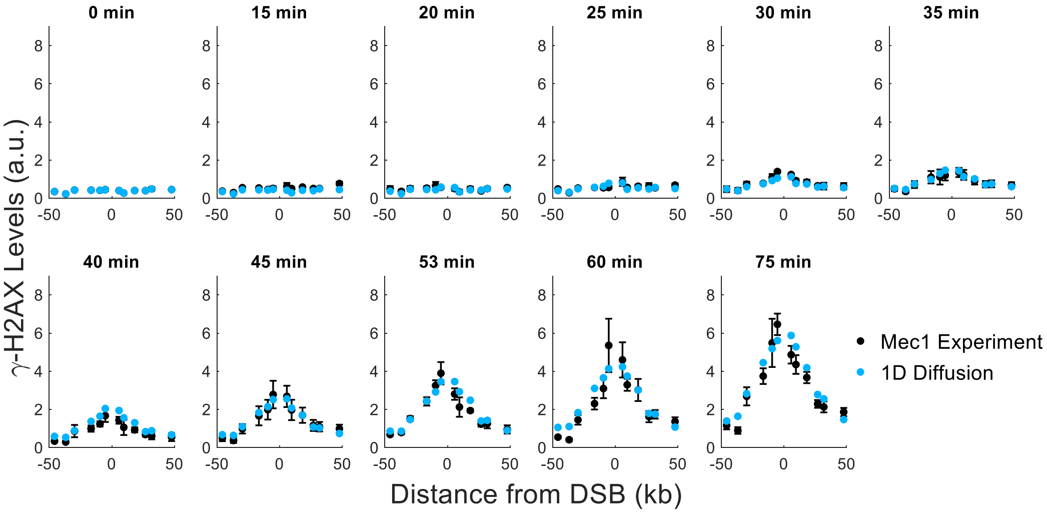

Figure S9: Comparison of experimental data by Mec1 to a 1D diffusion model with a constant rate of diffusion initiation. The best model parameters are C = 32, f = 0.28, N_{H2A} = 6, D = 22 kb^2/minute, k_{cat} = 1.9/minute, and k_{init} = 0.019/minute. For further details, refer to the caption of Figure S5.

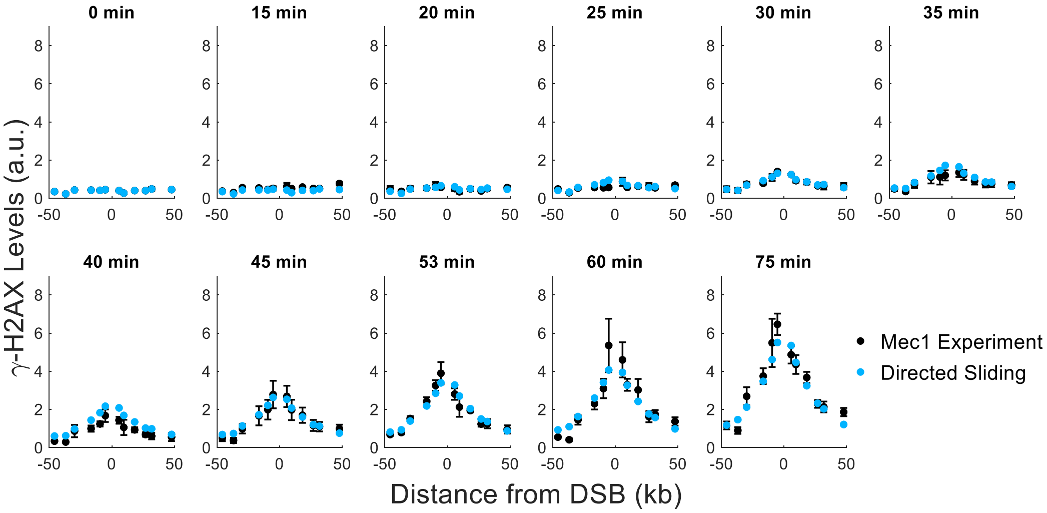

Figure S10: Comparison of experimental by Mec1 to a directed sliding model. The best model parameters are C = 73, f = 0.72, N_{H2A} = 2, k_{slide} = 17 kb/minute, k_{off} = 0.74/minute, and k_{init} = 0.0020/minute. For further details, refer to the caption of Figure S5.

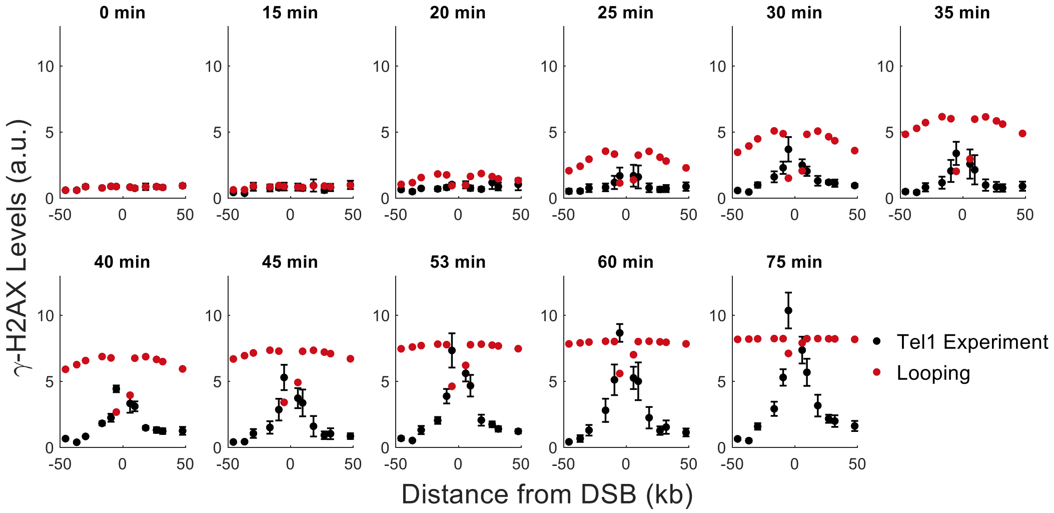

Figure S11: Comparison of experimental data by Tel1 to a looping model with a linearly increasing phosphorylation rate. The best model parameters are $C = 120$, $f = 0.035$, $N_{H2A} = 2$, $l = 8.4$ kb, and $\psi = 0.14/\text{minute}^2$. For further details, refer to the caption of Figure S5.

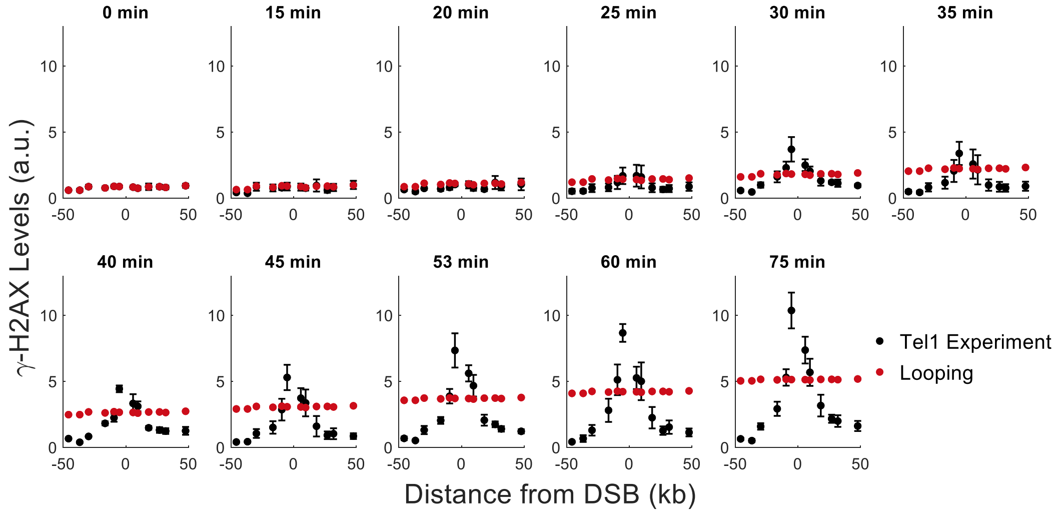

Figure S12: Comparison of experimental data by Tel1 to a looping model with a constant phosphorylation rate. The best model parameters are $C = 120$, $f = 0.035$, $N_{H2A} = 2$, $l = 8.4$ kb, $\varphi = 200$/minute, and $k_{init} = 0.017$/minute. The catalytic rate in the looping model (which is part of φ) is high, causing the H2As to become saturated. The flat profile increases over time as more of the cells in the population have kinases arrive to the break site. For further details and a discussion of the poor fit of the theory to the data, refer to the caption of Figure S5.

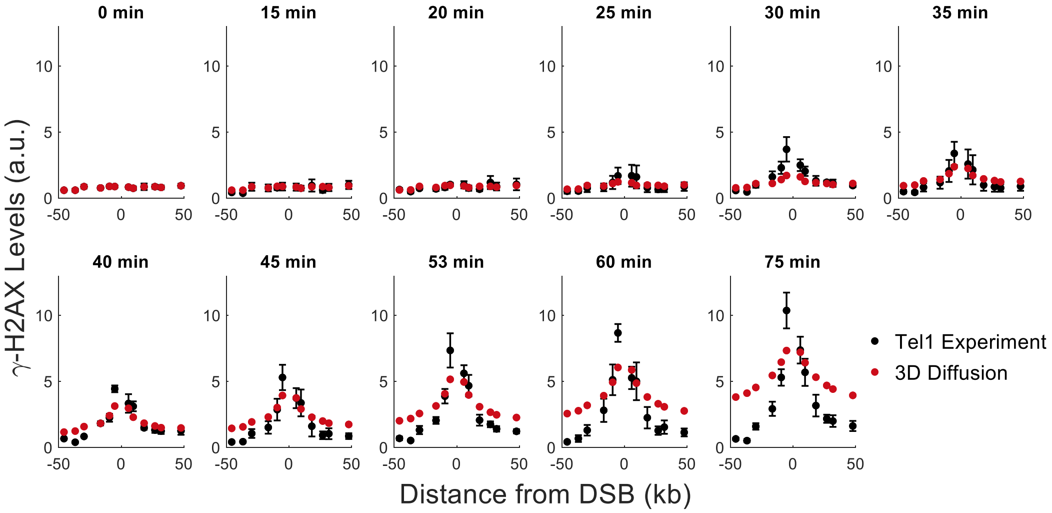

Figure S13: Comparison of experimental by Tel1 to a 3D diffusion model with a linearly increasing rate of diffusion initiation. The best model parameters are $C = 13$, $f = 0.16$, $N_{H2A} = 6$, $l = 15$ kb, and $\zeta = 6.2\times10^{-4}$/minute^2. For further details, refer to the caption of Figure S5.

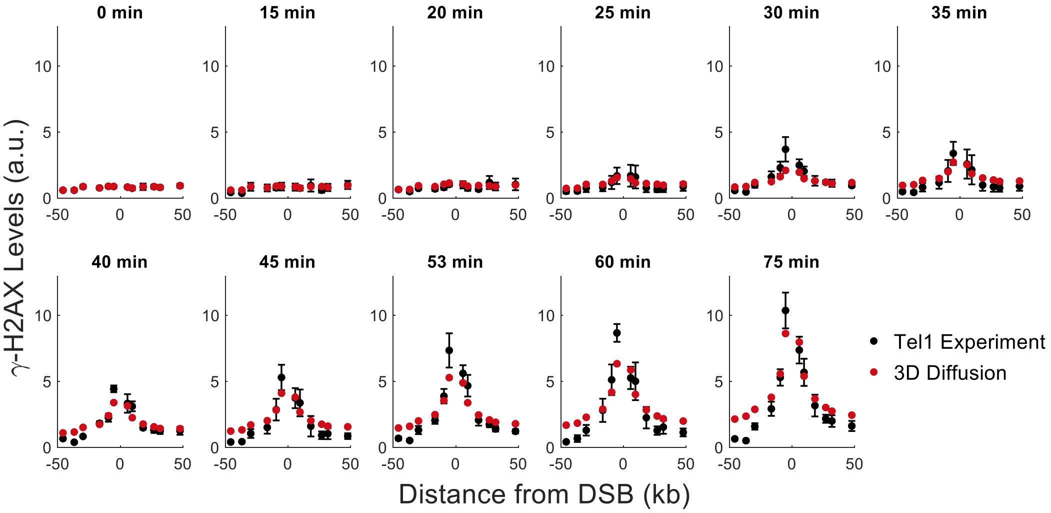

Figure S14: Comparison of experimental data by Tel1 to a 3D diffusion model with a constant rate of diffusion initiation. The best model parameters are $C = 73$, $f = 0.55$, $N_{H2A} = 6$, $l = 15$ kb, $\omega = 0.00030$/minute, and $k_{init} = 1.0$/minute. For further details, refer to the caption of Figure S5.

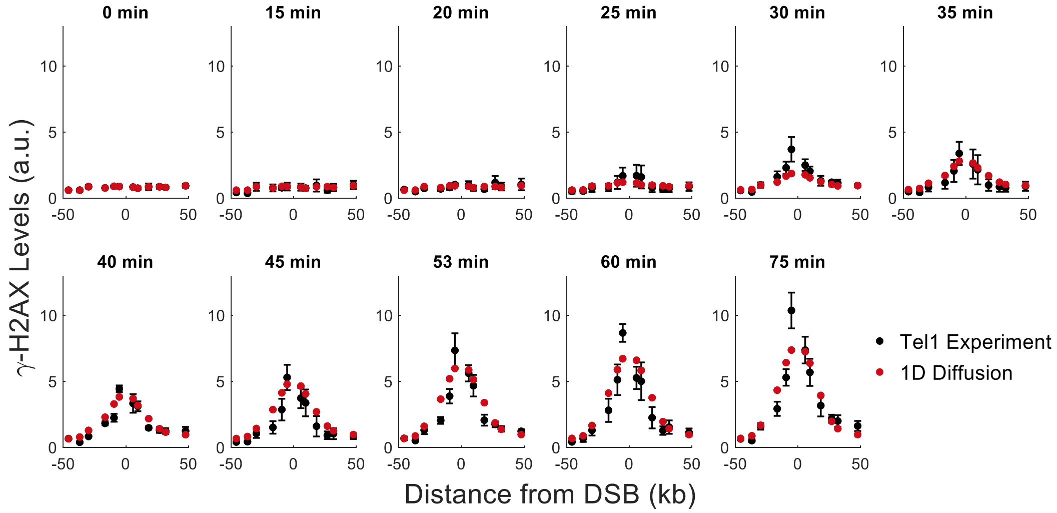

Figure S15: Comparison of experimental data by Tel1 to a 1D diffusion model with a linearly increasing rate of diffusion initiation. The best model parameters are $C = 9.3$, $f = 0.50$, $N_{H2A} = 4$, $D = 3.9$ kb^2/minute, $k_{cat} = 0.59$/minute, and $z = 37$/minute^2. For further details, refer to the caption of Figure S5.

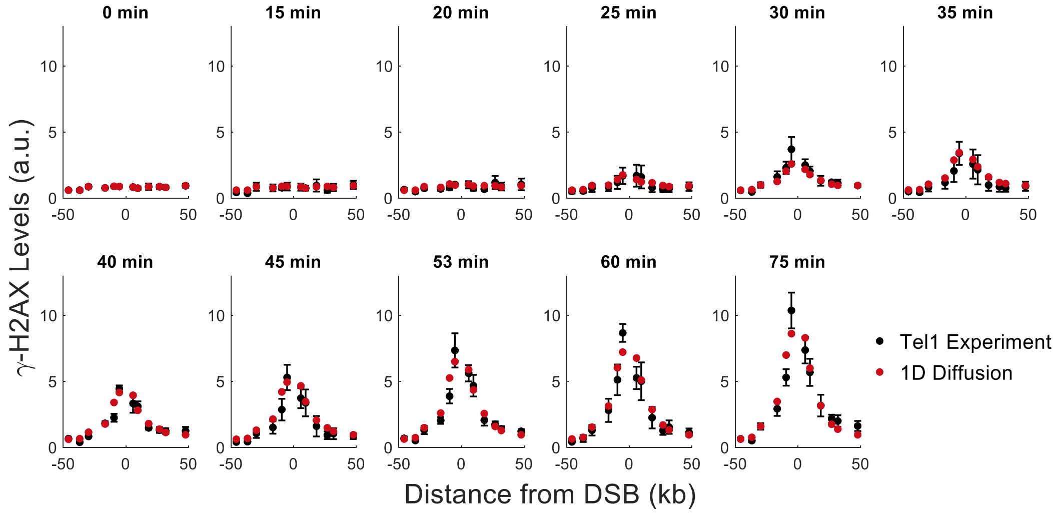

Figure S16: Comparison of experimental data by Tel1 to a 1D diffusion model with a constant rate of diffusion initiation. The best model parameters are $C = 32$, $f = 0.55$, $N_{H2A} = 4$, $D = 4.1$ kb^2/minute, $k_{cat} = 0.20$/minute, and $k_{init} = 0.098$/minute. For further details, refer to the caption of Figure S5.

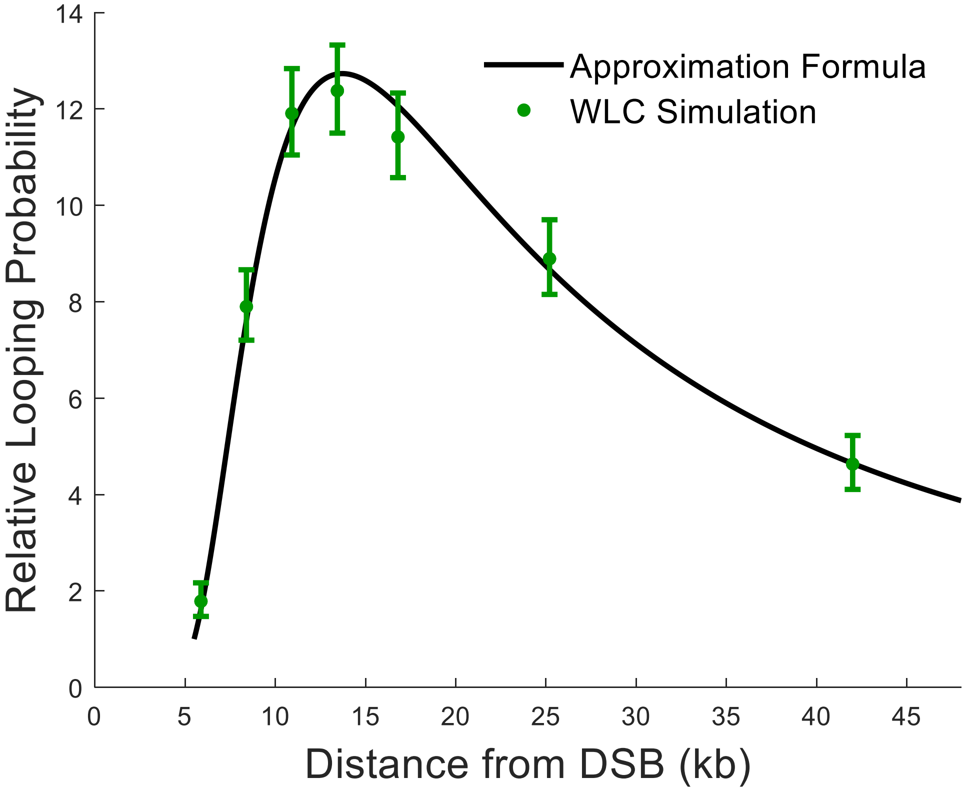

Figure S17: Relative looping probabilities for the worm-like chain model, assuming a Kuhn length of 8.4 kb. The worm-like chain model at thermodynamic equilibrium predicts the probability $P_{loop}(x)$ that the break site will come into physical contact with a locus *x* kb from the DSB is given by the approximation formula $P_{loop}(x) \propto x^{-3/2} e^{-2(x/l)^{-2}}$, shown by the black line. Shown in green are the results of a simulation of the exact worm-like chain model. The relative looping probabilities plotted here are $P_{loop}(x)$ normalized by $P_{loop}(x = 5.5 \text{ kb})$. The shape of P_{loop} is inconsistent with the shape of the experimental γ-H2AX profiles, which peak at 2 kb to 6 kb and then decreases as the distance from the break site increases. Here, we use a Kuhn length of *l* = 8.4 kb, which is the lower bound for the range of possible yeast chromatin Kuhn lengths determined by Arbona et al. (3). Note that if we were to use a higher Kuhn length, the predicted looping probability would peak at an even larger *x* and would therefore differ even more from the experimental γ-H2AX profile. Also note that P_{loop} function is an approximation that is inaccurate for small contour lengths, so we do not plot P_{loop} for x < 5.5 kb. For more information regarding P_{loop} and the worm-like chain simulation, see equation (11) and *Supplementary Information, Model Derivations, Looping Model Derivation*.

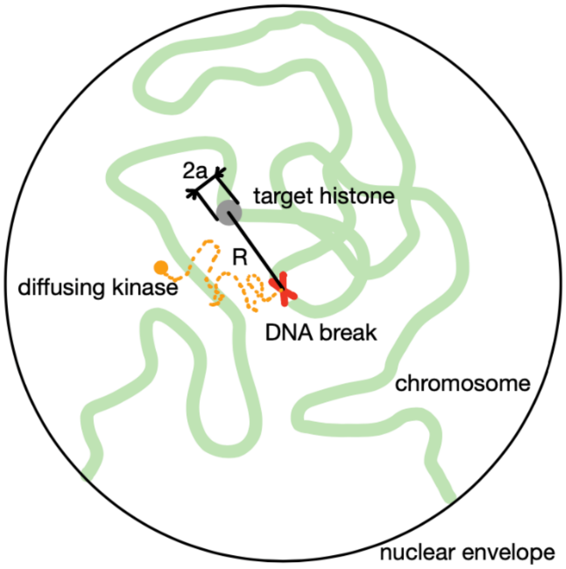
2a
target histone
R
diffusing kinase
DNA break
chromosome
nuclear envelope

Figure S18: Schematic of the 3D diffusion model of phosphorylation spreading

The kinase (orange) responsible for phosphorylating histone H2A (grey) diffuses from the break site (red). The histone target is modeled as an absorbing sphere of diameter *2a* located at a distance *R* from the break site. Assuming that *R* is much smaller than the radius of the nucleus, the probability of the kinase hitting the target histone before reaching the nuclear periphery (at which point we assume that the kinase only contributes to the background level of phosphorylation) is *a/R*.

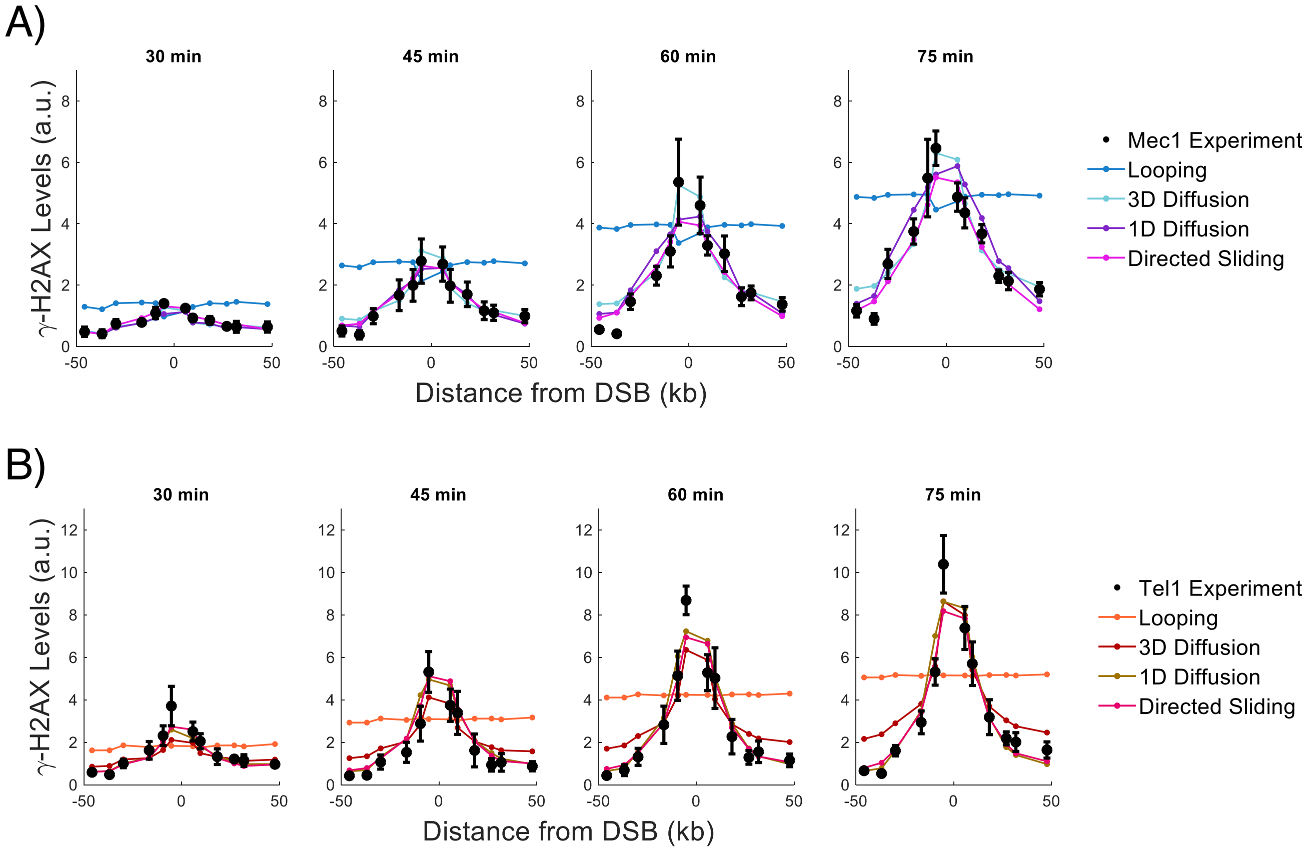

Figure S19: Comparison of all models to the experimental γ-H2AX profiles near the DSB. Plots show the best fits for the looping, 3D diffusion, 1D diffusion and directed sliding models on the same graph for easy comparison. These are the curves shown in Figures 4, S6, S9, S10, S12, S14, and S16. However, all fits to the Mec1 data and Tel1 data were performed separately in the *Supplementary Information*. For fair comparison of how well the models fit the data, we perform fits of the Mec1 3D diffusion and Tel1 directed sliding models independently of each other in the plots above (unlike in Figure 4 where Mec1 and Tel1 share the same values of the ChIP parameters C, f and N_{H2A}). The lines connecting the dots are shown to help visualize the curves and are not interpolation between the points. For a discussion of the poor fit for the looping model, refer to the captions of Figures S5 and S17. **(A)** Experimental and theoretical plots for Mec1. **(B)** Experimental and theoretical plots for Tel1. The experimental error bars represent the standard error of the mean from $n \geq 3$ measurements.

Supplemental Tables

Table S1: $\log_{10}$(Bayes Factor) for all mechanisms

The $\log_{10}$(Bayes Factor) is shown for every model variant. (Table 1 and 2 showed the Bayes factors for models with a constant rate of diffusion initiation or constant phosphorylation rate). The Bayes factor is calculated by dividing the probability of the indicated model by the probability of the best model. Bayes factors were computed for Mec1 and Tel1 separately. For Mec1, the best model is 3D diffusion with a constant rate of diffusion initiation. For Tel1, the best model is directed sliding.

Model	Mec1, $\log_{10}$(Bayes Factor)	Tel1, $\log_{10}$(Bayes Factor)
Looping with Linearly Increasing Phosphorylation Rate	-545	-449
Looping with Constant Phosphorylation Rate	-252	-251
3D Diffusion with Linearly Increasing Rate of Diffusion Initiation	-28	-136
3D Diffusion with Constant Rate of Diffusion Initiation	Best Model	-61
Directed Sliding	-14	Best Model
1D Diffusion with Linearly Increasing Rate of Diffusion Initiation	-28	-35
1D Diffusion with Constant Rate of Diffusion Initiation	-12	-5

Table S2: List of yeast strains used in this study

Strain	Genotype
JKM139	*MAT***a** *hml*Δ::*ADE1 hmr*Δ::*ADE1 ade1-100 leu2-3,112 lys5 trp1*::*hisG' ura3-52 ade3::GAL::HO*
yFD508	JKM139 *tel1*Δ::*TRP1 bar1*Δ::*ADE3*
yFD538	JKM139 *mec1*Δ::*NAT sml1*Δ::*KAN bar1*Δ::*ADE3*
yKL002	JKM139 *tel1*Δ::*TRP1 bar1*Δ::*ADE3 nej1*Δ::*HPH*
yKL003	JKM139 *mec1*Δ::*NAT sml1*Δ::*KAN bar1*Δ::*ADE3 nej1*Δ::*HPH*
yKL004	JKM139 *tel1*Δ::*TRP1 bar1*Δ::ADE3 *ku80*Δ::*HPH*
yKL005	JKM139 *mec1*Δ::*NAT sml1*Δ::*KAN bar1*Δ::ADE3 *ku80*Δ::*HPH*
yKL018	JKM139 *bar1*Δ::*ADE3 ku80*Δ::*HPH*
yKL019	yKL004 *GAL1-Ddc2* (plasmid PML105.45 integrated at *leu2-3,112*)
yKL025	yKL004 *hta1-S129A*
yKL026	yKL004 *hta2-S129A*
yKL040	yKL005 *hta2-S129A*
yKL041	yKL005 *hta1-S129A*
yKL046	yKL004 *rad9Δ*::*LEU2*
yKL047	yKL005 *rad9Δ*::*LEU2*

Table S3: Primers used during strain construction

Primer	Sequence
BL325	CTTCTCAAGAATTATAAGATGTTTT
BL326	ATCTTATAATTCTTGAGAAGGATCA
BL327	GAAGTCTGCCAAGGCTACCAAGGCTGCCCAAGAATTATAAGATCGGTTCTGGTATTTTAAAGAAGGCGGAAGGAACTAAA
BL329	TTACAGTTCTTGAGAAGCTTGTTTT
BL330	AAGCTTCTCAAGAACTGTAAGATCA
BL331	CAAAACTTGTTGCCAAAGAAGTCTGCCAAGACTGCCAAAGCTGCCCAAGAACTGTAAGAACTGAGTTGAAAAGAAACAAA
HPHorf+751	CAGAGCTTGGTTGACGGC
KL020	CAGCCAGTGGATCGTAAATA
KL021	ACAGTGCCCAATGAACCTAA
KL022	TCCGGTGGTAAAGGTGGTAA
KL023	ATTAACCTGGGGGCCATAAA
KL024	CAAAAGAAAGAGAGCCTAGCTG
ku80ORFL	CTCTTGAGTGTCTTTACCGC
KU80T2	CTAGTTCAGCAACCGAAATCC
ku80MX18	TAACGAGAGTGCAGGACATATGCACAAATAATATATCTCACACCATAATAGCATAGGCCACTAGTGGATCTG
ku80MX19	CTCTTTAACTGTGGTGACGAAAACATAACTCAAAGGATGTTAGACCTTTTCAGCTGAAGCTTCGTACGC
nej1-225	TCCAAAGACCTTTGGTCC
Nej1-MXp1	AGAATAACCATAACAACGGCCAGATAGGAGGTTAATCTTACACATGTGTGGATATCAAGCTTGCCTCGTCCCCGC
Nej1-MXp2	GAACTATTTGAAAGGTCCAACCTTAATTTTTGACGTTTAATTGACTTGCCGTCGACACTGGATGGCGGCGTTAGTATC
nej1+267	TTTACAGTGATGGCGAGC

Table S4: Plasmids used during strain construction

Plasmid	Genotype
pAG32	ampr, *HPH*
pBL13	ampr, *Cas9*, *URA3,* gRNA targeting *HTA1*
pBL14	ampr, *Cas9*, *URA3,* gRNA targeting *HTA2*
pJH2972	ampr, *Cas9*, *URA3*
PML105.45	*GAL1-Ddc2*, *LEU2*

Table S5: Primers used in quantitative PCR (qPCR)

Primer	Sequence
CTR86p1	CGGTCCTCGATTTTGTTACCTTC
CTR86p2	GCAAGGATATTCCTGCCTTTTTC
ERS1p1	ACACCCTGAATGGGGAAAC
ERS1p2	CTGCATGGGTGCTTGATG
HOCSp4	TCGTCAACCACTCTACAAAACCA
IMG1p1	TGGATCATGGACAAGGTCCTAC
IMG1p2	GGCGAAAACAATGGCACTCT
KL032	TGATGGTCATGGTGGTAGCG
KL033	CTTTGCGTCCAGAACAGACATAA
KL034	AAACAAACGACAGCATGCTGA
KL035	CTGGCCTCAGATCCTCGAA
KL036	CTCGCATAAAAAGCTGGAAGTG
KL037	ATCCAAAACCCTGGGCAAA
KL038	CCAAAAAGTAGTAAGGGAGAGGAT
KL039	ATAAACAGGGCCATATCGCATACA
KL040	TCATGTACTGTCCGGTGTGATT
KL041	ATCAAACTCCGTTTTTAGCCCC
Mak31p1	CCAAAGCGTCATGGACATCT
Mak31p2	AGGCCCATCATTCTACTACTGG
MAT1	ATTGCGACAAGGCTTCACCC
MAT2	CACATCACAGGTTTATTGGTTCCC
MAT3-1	ATGTCCTGACTTCTTTTGACGAGG
MAT4-1	ACGACCTATTTGTAACCGCACG
MAT9	GCCTCTATGTCCCCATCTTGTCTC
MAT10	GTGTTCCCGATTCAGTTTGACG
MAT13	TCAGGGTCTGGTGGAAGGAATG
MAT14	CAAAGGTGGCAGTTGTTGAACC
MAT15	CGTCTTCTCAGCGAACAACAGC
MAT16	GCAATAACCCACGGAAACACTG
MAT19	TCGTCGTCGCCATCATTTTC
MAT20	GCCCAAGTTTGAGAGAGGTTGC
MATYAp4	GATCTAAATAAATTCGTTTTCAATGATTAAAATAG
MT101-Pho5orf+50	CGCTTCTTTGGCCAATGC
MT102-Pho5orf+100	GGGTACCAATCTTGTCGAC
RAD18p1	TGTCATCGTTGGGACTGTCA

RAD18p2	GAAACATAACCATCCATCCTTTCC
YCR026Cp1	CACGCCTAGTTTCAGCTTGTTT
YCR026Cp2	CTTCAAGACATAATCAACGACGC
YCR043Cp1	CCAAGGAACTAATGATCTAAGCACA
YCR043Cp2	ACCAGCAGTAATAAGTCGTCCTGA
YCR061Cp1	GGAAAGACTGGCTCATCAAAAC
YCR061Cp2	ACATTCTCAGAGAGAACCTCCA

Supplemental Dataset

Dataset S1: γ-H2AX levels around MAT and RE

γ-H2AX levels are shown in the Excel file "Dataset S1." γ-H2AX levels were measured around the MAT locus for strains listed in Table S2. γ-H2AX measurements around RE were measured for strains yKL004 and yKL005.

References for Supplementary Information

1. C. I. White, J. E. Haber, Intermediates of recombination during mating type switching in Saccharomyces cerevisiae. *EMBO J.* **9**, 663–673 (1990).
2. B. Avşaroğlu, G. Bronk, K. Li, J. E. Haber, J. Kondev, Chromosome-refolding model of mating-type switching in yeast. *Proc. Natl. Acad. Sci. U. S. A.* **113**, E6929–E6938 (2016).
3. J.-M. Arbona, S. Herbert, E. Fabre, C. Zimmer, Inferring the physical properties of yeast chromatin through Bayesian analysis of whole nucleus simulations. *Genome Biol.* **18** (2017).
4. B. Avşaroğlu, *et al.*, Effect of Chromosome Tethering on Nuclear Organization in Yeast. *PLoS ONE* **9**, e102474 (2014).
5. H. Hajjoul, *et al.*, High-throughput chromatin motion tracking in living yeast reveals the flexibility of the fiber throughout the genome. *Genome Res.* **23**, 1829–1838 (2013).
6. Y. Zhang, O. K. Dudko, First-Passage Processes in the Genome. *Annu. Rev. Biophys.* **45**, 117–134 (2016).
7. J. Dekker, Mapping in Vivo Chromatin Interactions in Yeast Suggests an Extended Chromatin Fiber with Regional Variation in Compaction. *J. Biol. Chem.* **283**, 34532–34540 (2008).
8. J. Wilhelm, E. Frey, Radial Distribution Function of Semiflexible Polymers. *Phys. Rev. Lett.* **77**, 2581–2584 (1996).
9. E. Gobbini, *et al.*, Sae2 Function at DNA Double-Strand Breaks Is Bypassed by Dampening Tel1 or Rad53 Activity. *PLOS Genet.* **11**, e1005685 (2015).
10. M. Clerici, C. Trovesi, A. Galbiati, G. Lucchini, M. P. Longhese, Mec1/ATR regulates the generation of single-stranded DNA that attenuates Tel1/ATM signaling at DNA ends. *EMBO J.* **33**, 198–216 (2014).
11. H. Berg, *Random Walks in Biology*, New, expanded (Princeton University Press, 1993).
12. A. P. Singh, *et al.*, 3D Protein Dynamics in the Cell Nucleus. *Biophys. J.* **112**, 133–142 (2017).
13. J. Doye, Biophysical Chemistry, Applying polymer theory to biomolecules. *vdocuments.site* (April 13, 2020).
14. B. Avşaroğlu, G. Bronk, K. Li, J. E. Haber, J. Kondev, Chromosome-refolding model of mating-type switching in yeast. *Proc. Natl. Acad. Sci.* **113**, E6929–E6938 (2016).
15. J. Li, *et al.*, Regulation of Budding Yeast Mating-Type Switching Donor Preference by the FHA Domain of Fkh1. *PLoS Genet.* **8** (2012).

16. S. V. Kozlov, *et al.*, Autophosphorylation and ATM Activation ADDITIONAL SITES ADD TO THE COMPLEXITY. *J. Biol. Chem.* **286**, 9107–9119 (2011).

17. C. Arnould, *et al.*, Loop extrusion as a mechanism for DNA Double-Strand Breaks repair foci formation. *bioRxiv*, 2020.02.12.945311 (2020).

18. K. Brogaard, L. Xi, J.-P. Wang, J. Widom, A map of nucleosome positions in yeast at base-pair resolution. *Nature* **486**, 496–501 (2012).

19. J.-A. Kim, M. Kruhlak, F. Dotiwala, A. Nussenzweig, J. E. Haber, Heterochromatin is refractory to γ-H2AX modification in yeast and mammals. *J. Cell Biol.* **178**, 209–218 (2007).

20. D. S. Sivia, J. Skilling, *Data analysis: a Bayesian tutorial*, 2nd ed (Oxford University Press, 2006).